In vitro and in vivo evaluation of the bifunctional chelator NODIA-Me in combination with a prostate-specific membrane antigen targeting vector

Läppchen, Tilman ; Kiefer, Yvonne ; Holland, Jason P ; Bartholomä, Mark D

Abstract: Introduction We recently developed a chelating platform based on the macrocycle 1,4,7-triazacyclononane with up to three five-membered azaheterocyclic arms for complexation of the PET nuclides gallium-68 and copper-64. The main objective of this study was to evaluate the stability and pharmacokinetics of 68Ga- and 64Cu-complexes of the bifunctional chelator NODIA-Me 1 covalently bound to a PSMA targeting vector in vivo. Methods NODIA-Me 1 was conjugated to the PSMA targeting Glu-NH-CO-NH-Lys moiety to give the bioconjugate NODIA-Me-NaI-Ahx-PSMA 4. The stability of [68Ga]4 and [64Cu]4 was assessed in vitro by serum stability studies. The PSMA binding affinity was determined in competitive cell experiments in LNCaP cells using 68Ga-PSMA-HBED-CC as radioligand. The stability and pharmacokinetics of [68Ga]4 and [64Cu]4 was evaluated by PET imaging and ex vivo biodistribution studies in mice bearing subcutaneous LNCaP tumors. Results In human serum, [68Ga]4 and [64Cu]4 remained intact to 85% (3 h) and 92% (24 h), respectively. Nature of the metal chelate influenced PSMA binding affinity with IC50 of 233 ± 10 nM for uncomplexed 4, 681 ± 7 nM for Cu-4 and 176 ± 10 nM for Ga-4. In animal studies, [68Ga]4 and [64Cu]4 revealed low uptake (1% IA g−1) in the majority of organs. Kidney uptake at 1 h p.i. was 6.28 ± 0.92% IA g−1 and 4.96 ± 0.79% IA g−1 and specific tumor uptake was 1.33 ± 0.46% IA g−1 and 2.15 ± 0.38% IA g−1 for [68Ga]4 and [64Cu]4, respectively. Conclusion The bifunctional chelator NODIA-Me 1 was successfully conjugated to a PSMA targeting moiety. In small-animal PET imaging and ex vivo biodistribution studies, 68Ga- and 64Cu-labelled conjugates specifically delineated PSMA-positive LNCaP tumors and exhibited rapid renal clearance from non-target tissues with no significant demetallation/transchelation in vivo. The results support further development of this novel chelating platform for production of 68Ga- and 64Cu-labelled radiopharmaceuticals.

DOI: https://doi.org/10.1016/j.nucmedbio.2018.03.002

Läppchen, Tilman; Kiefer, Yvonne; Holland, Jason P; Bartholomä, Mark D (2018). In vitro and in vivo evaluation of the bifunctional chelator NODIA-Me in combination with a prostate-specific membrane antigen targeting vector. Nuclear medicine and biology, 60:45-54.
DOI: https://doi.org/10.1016/j.nucmedbio.2018.03.002

In vitro and in vivo evaluation of the bifunctional chelator NODIA-Me in combination with a prostate-specific membrane antigen targeting vector

Tilman Läppchen[1,2], Yvonne Kiefer[1], Jason P. Holland[1,3], and Mark D. Bartholomä[1,*]

[1] Department of Nuclear Medicine, Medical Center – University of Freiburg, Faculty of Medicine, University of Freiburg, Hugstetterstrasse 55, D-79106, Freiburg, Germany

[2] Department of Nuclear Medicine, Inselspital, Bern University Hospital and University of Bern, Freiburgstrasse, CH-3010 Bern, Switzerland

[3] Department of Chemistry, University of Zürich, Winterthurerstrasse 190, CH-8057, Zürich, Switzerland

*** Corresponding Author:**

Dr. Mark D. Bartholomä

Tel: +49-(761)-270-39600

Fax: +49-(761)-270-39300

E-mail: mark.bartholomae@uniklinik-freiburg.de

Key words: Gallium-68, Copper-64, prostate-specific membrane antigen (PSMA), PET imaging, bifunctional chelator.

Running Title: NODIA-Me-PSMA

Abstract

Introduction: We recently developed a chelating platform based on the macrocycle 1,4,7-triazacyclononane with up to three five-membered azaheterocyclic arms for complexation of the PET nuclides gallium-68 and copper-64. The main objective of this study was to evaluate the stability and pharmacokinetics of ^{68}Ga- and ^{64}Cu-complexes of the bifunctional chelator NODIA-Me **1** covalently bound to a PSMA targeting vector *in vivo*.

Methods: NODIA-Me **1** was conjugated to the PSMA targeting Glu-NH-CO-NH-Lys moiety to give the bioconjugate NODIA-Me-NaI-Ahx-PSMA **4**. The stability of [^{68}Ga]**4** and [^{64}Cu]**4** was assessed *in vitro* by serum stability studies. The PSMA binding affinity was determined in competitive cell experiments in LNCaP cells using ^{68}Ga-PSMA-HBED-CC as radioligand. The stability and pharmacokinetics of [^{68}Ga]**4** and [^{64}Cu]**4** was evaluated by PET imaging and *ex vivo* biodistribution studies in mice bearing subcutaneous LNCaP tumors.

Results: In human serum, [^{68}Ga]**4** and [^{64}Cu]**4** remained intact to 85% (3 h) and 92% (24 h), respectively. Nature of the metal chelate influenced PSMA binding affinity with IC_{50} of 233 ± 10 nM for uncomplexed **4**, 681 ± 7 nM for Cu-**4** and 176 ± 10 nM for Ga-**4**. In animal studies, [^{68}Ga]**4** and [^{64}Cu]**4** revealed low uptake (≤1% IA g^{-1}) in the majority of organs. Kidney uptake at 1 h p.i. was 6.28 ± 0.92% IA g^{-1} and 4.96 ± 0.79% IA g^{-1} and specific tumor uptake was 1.33 ± 0.46% IA g^{-1} and 2.15 ± 0.38% IA g^{-1} for [^{68}Ga]**4** and [^{64}Cu]**4**, respectively.

Conclusion: The bifunctional chelator NODIA-Me **1** was successfully conjugated to a PSMA targeting moiety. In small-animal PET imaging and *ex vivo* biodistribution studies, ^{68}Ga- and ^{64}Cu-labelled conjugates specifically delineated PSMA-positive LNCaP tumors and exhibited rapid renal clearance from non-target tissues with no significant demetallation/transchelation *in vivo*. The results support further development of this novel chelating platform for production of ^{68}Ga- and ^{64}Cu-labelled radiopharmaceuticals.

1. Introduction

Obtaining maximum information from positron emission tomography (PET) imaging relies on the development of target-specific radiotracers. Besides compounds labelled with the PET nuclides carbon-11 and fluorine-18, radiopharmaceuticals labelled with positron-emitting radiometals are an important part of ongoing research. In particular, the two radiometals gallium-68 and copper-64 have received increased attention in the development of new PET radiopharmaceuticals. One general advantage over carbon-11 and fluorine-18 is that labelling reactions using radiometals can typically be carried out in aqueous media and are therefore amenable to kit formulations. The interest in gallium-68 originates from its physical properties ($t_{1/2}$ = 67.71 min, β^+ 89%, $E(\beta^+)_{max}$ = 1.9 MeV), which are suitable for use with targeting vectors possessing rapid pharmacokinetics such as radiotracers based on small molecules and peptides [1-4]. In contrast to carbon-11 and fluorine-18, the radiometal gallium-68 is generator produced and readily accessible without the need for an on-site cyclotron. More recently, a GMP-compliant pharmaceutical grade generator produced by Eckert & Ziegler has received marketing authorization. Other clinical grade gallium-68 generators are in development, which will spur the continued use of ^{68}Ga-based radiopharmaceuticals in the near future [5].

The cyclotron-produced radiometal copper-64 has also shown promise as both a suitable PET imaging and a therapeutic radionuclide due to its favorable decay characteristics ($t_{1/2}$ = 12.7 h, β^+ 17.4%, $E(\beta^+)_{max}$ = 0.656 MeV; β^- 39%, $E(\beta^-)_{max}$ = 0.573 MeV) and commercial availability in large quantities with high specific activity [6-8]. The intermediate half-life of copper-64 allows visualization of processes at time points up to 48 h, which is ideal for developing radiopharmaceuticals that require longer circulation times to achieve optimal uptake. The half-life of copper-64 also allows central production and shipment. Furthermore, ^{64}Cu-labelled radiopharmaceuticals may be used to provide pharmacokinetic

profiles of therapeutic radiotracers that are labelled with copper-67 ($t_{1/2}$ = 61.5 h, β^- 100%, E_{max} = 0.121 MeV) as this isotope has promise in endoradiotherapy applications [9].

Radiolabelling of target-specific radiopharmaceuticals with a radiometal generally requires the use of a bifunctional chelator (BFC) that (1) forms kinetically stable complexes with the radiometal and (2) possesses a function for the covalent attachment of a target-specific molecule. High kinetic and metabolic stability of the metal chelate is essential to avoid accumulation of radioactivity in background tissues that may result from degradation or transmetallation *in vivo*. However, introduction of a metal chelate into a biomolecule is a non-innocent modification. Chelates/metal complexes often have an impact on the biological properties of the radiopharmaceutical. The use of different radiometals with the same BFC can alter binding affinities as illustrated by reported studies on various gallium and yttrium labelled somatostatin analogs such as DOTA-[Tyr^3]-octreotate and DOTA-octreotide [10]. Variation of the metal chelate by using different BFCs with the same radiometal can also result in altered pharmacokinetic profiles [11-12]. Interestingly, the influence of the metal chelate is not limited to radiotracers based on small molecules or peptides. For example, the biodistribution profiles of ^{64}Cu-labelled antibody fragments as well as full antibody conjugates can also be influenced by the nature of the metal chelate [13-14]. Evidently the important role that chemical structure has on the biological performance of a radiotracer demands continued development and optimization of new BFCs. The dependency of radiotracer performance on the chemical structure also presents an opportunity for radiochemists to tune the pharmacokinetics. Radiotracer design incorporates control over the metal complex properties such as overall charge, lipophilicity and size as indispensable handles for optimizing target-specific binding and distribution *in vivo*.

Numerous BFCs have been developed for both gallium-68 and copper-64 (Scheme 1), such as NOTA (1,4,7-triazacyclononane-1,4,7-triacetic acid), NODAGA (1,4,7-

triazacyclononane-1-glutaric acid-4,7-diacetic acid) [15-18] [1, 11, 19-21], TRAP (1,4,7-triazacyclononane-1,4,7-tris[methyl(2-carboxyethyl)phosphinic acid) [22-24], PCTA (3,6,9,15-tetraazabicyclo[9.3.1]pentadeca-1(15),11,13-triene-3,6,9-triacetic acid) [25-27], and rigid cage-like sarcophagine type ligands such as diamsar [3, 28-32]. The most prominent BFC for gallium-68 is the ligand DOTA (1,4,7,10-tetraazacyclododecane-1,4,7,10-tetraacetic acid [6], while copper-specific ligands include CB-TE2A (2,2'-(1,4,8,11-tetraazabicyclo[6.6.2]hexadecane-4,11-diyl)diacetic acid) [28, 33-38], and bispidines [39-41]. For a more comprehensive overview, the reader is referred to recent reviews [6, 42-45].

The clinical success of ^{68}Ga-labelled PSMA-HBED-CC (also known as DKFZ-PSMA-11) represents an archetypal example of a system where the nature of the metal chelate forms an integral part of the radiotracer's binding mode. The aromatic rings of the [^{68}Ga]Ga-HBED-CC chelate form a key element for docking hydrophobic patches near the binding pocket of the target protein prostate-specific membrane antigen (PSMA) [46]. PSMA is an attractive molecular target for the diagnosis due to its upregulation in primary and metastatic prostate cancer [47-48]. The PSMA pocket is comprised of two sub-pockets with one surface-exposed highly positively charged pharmacophore region containing two Zn^{2+} ions, and a second buried hydrophobic non-pharmacophore sub-pocket [49-50]. While the urea motif of PSMA-HBED-CC binds to the pharmacophore region, the BFC HBED-CC interacts advantageously with the lipophilic part of the PSMA pocket [46, 51]. In case of traditional macrocyclic BFCs like DOTA, which lack aromatic rings, lipophilic substituents were consequently introduced into the linker region in order to mimic the proven additional biologic interactions of the chelator HBED-CC [52-56].

We recently described a chelating platform based on the macrocycle 1,4,7-triazacyclononane (TACN) with additional five-membered azaheterocyclic arms including imidazole, methylimidazole and thiazole residues [57]. These ligands are characterized by

their excellent complexation properties for radioactive, divalent copper cations. They label instantaneously with [^{64}Cu]$CuCl_2$ under very mild conditions in the pH range of 4 – 8 with high molar activities of 120 – 180 MBq nmol^{-1}. Experiments showed that corresponding methylimidazole-type ligands (e.g. NODIA-Me in Scheme 1) that incorporate borderline azaheterocyclic N donors according to the HSAB (hard and soft acids and bases) principle form rigid and stable Ga^{3+} complexes allowing their application also with the PET-nuclide gallium-68 [58]. This study reports the *in vitro* and *in vivo* evaluation of the BFC NODIA-Me (2-(4,7-bis((1-methyl-1H-imidazol-2-yl)methyl)-1,4,7-triazonan-1-yl)acetic acid) **1** labelled with gallium-68 and copper-64 in combination with the glutamate-urea-lysine moiety for targeting PSMA. The aim of this study was to demonstrate that NODIA-Me is suitable for future radiopharmaceutical development.

2. Materials and Methods

2.1. General

Chemicals and solvents were purchased from Sigma-Aldrich and TCI Europe, and used as received. The precursor Glu-NH-CO-NH-Lys(Ahx)-$(tBu)_3$ ester was purchased from ABX (Radeberg, Germany). Fmoc-3-(2-naphthyl)-L-alanine was obtained from IRIS Biotech (Marktredwitz, Germany). The bifunctional chelator NODIA-Me (2-(4,7-bis((1-methyl-1H-imidazol-2-yl)methyl)-1,4,7-triazonan-1-yl)acetic acid) **1** was prepared as previously described [58]. The radiotracer [^{68}Ga]Ga-PSMA-HBED-CC was prepared as previously described [59]. Low resolution electrospray ionisation mass spectrometry (LR-ESI(+)-MS) was performed on a PerkinElmer Flexar SQ 300 MS Detector. High resolution mass spectrometry (HR-ESI(+)-MS) was performed on a Thermo Scientific Exactive mass spectrometer. ^{1}H and ^{13}C NMR spectra were measured in D_2O at room temperature using a Bruker Avance III HD 500MHz NMR spectrometer (Rheinstetten, Germany). Chemical shifts are given in parts per million (ppm) and are reported relative to 4,4-dimethyl-4-silapentane-1-sulfonic acid (DSS). Coupling constants are reported in hertz (Hz). The multiplicity of the NMR signals is described as follows: s = singlet, d = doublet, t = triplet, q = quartet, m = multiplet. Radiolabelling with [^{68}Ga]$GaCl_3$ was accomplished using a fully automated synthesis module (Pharmtracer, Eckert & Ziegler, Berlin, Germany) with an IGG100 generator (Eckert & Ziegler, Berlin, Germany). [^{64}Cu]$CuCl_2$ was purchased from the Department of Preclinical Imaging and Radiopharmacy of the Eberhard-Karls-University (Tübingen, Germany). [^{64}Cu]$CuCl_2$ was produced via the ^{64}Ni(p,n)^{64}Cu route. The corresponding molar activity was 300–400 MBq nmol^{-1} (18 h EOB). High performance liquid chromatography (HPLC) was conducted on an Agilent 1260 Infinity System equipped with an Agilent 1200 DAD UV detector (UV detection at 220 nm) and a gamma-radiation detector (Ramona, Raytest GmbH, Straubenhardt, Germany) in series. A Phenomenex Jupiter Proteo

(250 × 4.60 mm) column was used for analytical HPLC. The solvent system was A = H_2O (0.1% TFA) and B = acetonitrile (0.1% TFA). The gradient was 0–1 min 5% B, 1–20 min 5–40% B at a flow rate of 1 mL min^{-1}. Semi-preparative HPLC was performed on a Knauer Smartline 1000 HPLC system in combination with a Macherey Nagel VP 250/21 Nucleosil 120-5 C18 column. Conditions A were 0–40 min 5–60% B at a flow rate of 12 mL min^{-1}. Conditions B were 0–25 min 5–95% B at a flow rate of 12 mL min^{-1}. Samples were lyophilized using a Christ Alpha 1-2 LD plus lyophilizer. All instruments measuring radioactivity were calibrated and maintained in accordance with previously reported routine quality-control procedures [60]. Radioactivity was measured using an Activimeter ISOMED 2010 (Nuklear-Medizintechnik, Dresden, Germany). For accurate quantification of radioactivity, experimental samples were counted for 1 min on a calibrated PerkinElmer (Waltham, MA) 2480 Automatic Wizard Gamma Counter by using a dynamic energy window of 400–600 keV for gallium-68 and copper-64 (511 keV emission). A Thermo Fisher Heraeus Fresco 21 centrifuge was used for centrifugation.

2.2. Bioconjugate Synthesis

*2.2.1. Glu-NH-CO-NH-Lys(Ahx-NaI)-$(tBu)_3$ ester (**2**)*

Fmoc-L-2NaI-OH (Fmoc-3-(2-naphthyl)-L-alanine) (16.6 mg, 0.038 mmol), HATU (1-[bis(dimethylamino)methylene]-1*H*-1,2,3-triazolo[4,5-b]pyridinium-3-oxide hexafluorophosphate) (14.5 mg, 0.038 mmol) and DIPEA (*N*,*N*-diisopropylethylamine) (9.8 mg, 14 µL, 0.076 mmol) were mixed in 500 µL anhydrous *N*,*N*-dimethylformamide (DMF) and allowed to stir for 1 h at r.t.. Then, Glu-NH-CO-NH-Lys(Ahx)-$(tBu)_3$ (20.7 mg, 0.034 mmol) in 100 µL DMF was added and stirring was continued for additional 16 h. The solvent was removed by rotary evaporation and the residue treated with 20% piperidine/DMF for 30 min at r.t.. After removal of the solvent, the residue was taken up in water/acetonitrile (50:50

v/v) with 0.1 % trifluoroacetic acid (TFA) and purified by semi-preparative HPLC. Fractions containing the product were combined and lyophilized to give compound **2** as white powder (26.3 mg, 0.033 mmol, 97%). LR-ESI-MS calcd m/z for $C_{43}H_{68}N_5O_9$ (M + H): 798.5, found: 799.1. HR-ESI-MS calcd m/z for $C_{43}H_{68}N_5O_9$ (M + H): 798.5012, found: 798.5007. RP-HPLC (semi-preparative, conditions A): t_R = 44 min.

*2.2.2. NODIA-Me-NaI-Ahx-PSMA-(tBu)$_3$ ester (**3**)*

NODIA-Me (13.6 mg, 0.036 mmol), HATU (15.2 mg, 0.040 mmol) and DIPEA (10.3 mg, 14 µL, 0.080 mmol) were mixed in 500 µL anhydrous DMF and allowed to stir for 30 min at r.t. Then, compound **2** (26.3 mg, 0.033 mmol) in 100 µL DMF was added and stirring was continued for additional 16 h. The solvent was removed by rotary evaporation and the residue was taken up in water/acetonitrile (50:50 v/v) with 0.1 % TFA and purified by semi-preparative HPLC. Fractions containing the product were combined and the solvent removed by rotary evaporation to give compound **3** as colorless solid (26.5 mg, 0.023 mmol, 70%). LR-ESI-MS calcd m/z for $C_{61}H_{95}N_{12}O_{10}$ (M + H): 1155.7, found: 1156.3. HR-ESI-MS calcd m/z for $C_{61}H_{95}N_{12}O_{10}$ (M + H): 1155.7289, found: 1155.7301. RP-HPLC (semi-preparative, conditions B): t_R = 25 min.

*2.2.3. NODIA-Me-NaI-Ahx-PSMA (**4**)*

Compound **3** (26.5 mg, 0.023 mmol) was dissolved in 1 mL 5 M hydrochloric acid and allowed to stir for 16 h at room temperature. The reaction mixture was concentrated by rotary evaporation to a volume of 1 mL and further purified by semi-preparative HPLC to give NODIA-Me-NaI-Ahx-PSMA ((4*S*,18*S*,22*S*)-1-(4,7-bis((1-methyl-1*H*-imidazol-2-yl)methyl)-1,4,7-triazonan-1-yl)-4-(naphthalen-2-ylmethyl)-2,5,12,20-tetraoxo-3,6,13,19,21-pentaazatetracosane-18,22,24-tricarboxylic acid) **4** as colorless powder after lyophilization

(20.6 mg, 0.021 mmol, 91%). ^{1}H-NMR (D2O, pD ≤ 2): δ = 7.79 – 7.73 (4H, m), 7.48 – 7.45 (4H, m), 7.42 (1H, d, *J* = 1.7), 7.33 (2H, s), 4.89 (1H, dd, *J* = 10.7, 4.7), 4.21 (3H, m), 4.06 – 3.95 (3H, m), 3.69 (3H, s), 3.67 (3H, s), 3.47 (2H, m), 3.36 – 3.28 (4H, m), 3.12 – 2.94 (7H, m), 2.80 (1H, m), 2.67 (1H, d, *J* = 16), 2.53 (1H, m), 2.54 (4H, m), 2.43 (1H, m), 2.12 (3H, m), 2.01 (1H, m), 1.92 (1H, m), 1.67 (1H, m), 1.55 (1H, m), 1.49 – 1.38 (6H, m), 1.26 (2H, m), 1.15 (2H, m). ^{13}C-NMR (D2O, pD ≤ 2): δ = 177.2, 176,7, 176.2, 171.5, 165.0, 163.0 (q, TFA), 159.2, 142.6, 134.8, 133.0, 132.0, 128.2, 128.1, 127.9, 127.4, 127.2, 126.8, 126.3, 124.2, 124.1, 118.8, 118.6, 116.3 (q, TFA), 56.4, 55.9, 53.3, 53.2, 52.6, 51.6, 50.0, 48.4, 47.8, 47.0, 45.3, 39.3, 39.0, 35.6, 34.4, 30.5, 30.0, 28.0, 27.8, 26.3, 25.4, 24.9, 22.3. LR-ESI-MS calcd m/z for $C_{49}H_{71}N_{12}O_{10}$ (M + H): 987.5, found: 987.7. HR-ESI-MS calcd m/z for $C_{49}H_{71}N_{12}O_{10}$ (M + H): 987.5411, found: 987.5399. RP-HPLC (semi-preparative, conditions B): t_R = 14 min; RP-HPLC (analytical, UV: 220 nm): t_R = 15:20 min.

2.3. Preparation of non-radioactive references

For each reference compound, the bioconjugate **4** (500 µg, 0.51 µmol) in 250 µL H_2O was mixed with 250 µL of metal stock solutions containing 1.5 equivalents of the corresponding metal salt ($CuCl_2$·2 H_2O, $Ga(NO_3)_3$ hydrate) and heated at 95 °C for 15 min. After cooling to r.t., the complexes were purified using C_{18} Sep Pak cartridges, which were preconditioned with EtOH and H_2O (5 mL each). After loading, the cartridge was washed with H_2O (2 mL) and the product was eluted off using EtOH:H_2O (50:50 v/v; 2mL). After evaporation of EtOH at ambient temperature, samples were lyophilized to give Cu-**4** (479 µg, 0.46 µmol, 90%) and Ga-**4** (461 µg, 0.44 µmol, 86%). HR-ESI-MS of Cu-**4** calcd m/z for $C_{49}H_{69}CuN_{12}O_{10}^{+}$ (M – H): 1048.4550, found: 1048.4551. RP-HPLC of Cu-**4** (analytical, UV: 220 nm): t_R = 17:42 min. HR-ESI-MS of Ga-**4** calcd m/z for $C_{49}H_{68}GaN_{12}O_{10}^{+}$ (M – 2H): 1053.4432, found: 1053.4426. RP-HPLC of Ga-**4** (analytical, UV: 220 nm): t_R = 15:33 min.

2.4. Radiolabelling

*2.4.1. Radiosynthesis of [^{68}Ga]Ga-NODIA-Me-NaI-Ahx-PSMA ([^{68}Ga]**4**)*

^{68}Ga radiolabelling was accomplished by using the Modular-Lab PharmTracer automated synthesis module (Eckert&Ziegler, Berlin, Germany) as previously described [58]. The reaction vial contained 20 µg of **4** in a mixture of 400 µL sodium acetate buffer (pH 4.5) and 2 mL water. Radiolabelling was performed at 95°C for 10 min. The radiochemical purity (RCP) was >98% and the decay corrected radiochemical yield (RCY) was >98%. The mean molar activity was A_m = 20.2 ± 2.3 MBq nmol^{-1} (*n* = 10). RP-HPLC (analytical, radioactivity detector): t_R ([^{68}Ga]**4**) = 15:50 min.

*2.4.2. Radiosynthesis of [^{64}Cu]Cu-NODIA-Me-NaI-Ahx-PSMA ([^{64}Cu]**4**)*

Radiolabelling with [^{64}Cu]$CuCl_2$ was accomplished by dissolving 6 µg (6 nmol) of **4** in 200 µL ammonium acetate (0.1 M, pH 8.2) followed the addition of ~120 MBq [^{64}Cu]$CuCl_2$ in 0.1 M HCl. The solution was then incubated for 15 min at r.t. The RCP was >99% and the decay corrected RCY was >99%. The mean molar activity was A_m = 20.5 ± 1.8 MBq nmol^{-1} (n = 5). RP-HPLC (analytical, radioactivity detector): t_R ([^{64}Cu]**4**) = 17:43 min.

2.5. Lipophilicity (log $D_{oct/PBS}$) measurements

For log $D_{oct/PBS}$ measurements, 1–2 MBq of [^{68}Ga]**4**, [^{64}Cu]**4** and [^{68}Ga]Ga-PSMA-HBED-CC (20 µL) were added to a pre-saturated mixture of phosphate buffered saline pH 7.4 (PBS) (480 µL) and octanol (500 µL). Samples were shaken for 30 min at room temperature, centrifuged at 21,100 g for 5 min and 100 µL of each phase were counted using a Packard Cobra gamma counter. Experiments were performed in triplicate.

2.6. Serum stability measurements

For each experiment, 5–10 MBq (50 µL) of [^{68}Ga]**4** and [^{64}Cu]**4** were added to human serum (500 µL, human male AB plasma, Sigma-Aldrich), which was pre-equilibrated at 37 °C in a cell incubator for 1 h. Samples were vortexed briefly and stored at 37 °C in a cell incubator. At selected time points, 100 µL aliquots were taken from the serum solution and serum proteins removed by centrifugation using centrifuge tubes (molecular weight cutoff 30 kDa) at 4,000 g for 5 min at 4 °C. 100 µL PBS were added to the filter followed by an additional centrifugation step. For determination of protein bound fraction, the filters and the filtrates were transferred into plastic tubes, and samples were counted using a Packard Cobra gamma counter. A sample of the filtrate was kept on ice until HPLC analysis. The percentage of intact [^{68}Ga]**4** and [^{64}Cu]**4** was calculated from the HPLC chromatograms. All experiments were performed in triplicate.

2.7. Cell culture

PSMA-positive LNCaP cells (ATCC, Manassas, VA, USA) were cultured at 37 °C in a 5% CO_2 atmosphere (RPMI Medium 1640 GlutaMAX containing 10% FBS, 1% 100 U mL^{-1} penicillin and 100 µg mL^{-1} streptomycin, 1% sodium-pyruvate 1 mM, 1% L-glutamin 2 mM).

2.8. Competitive binding assay

The binding affinity of the bioconjugate **4** and the corresponding metallated compounds Ga-**4** and Cu-**4** was determined using a cell-based competitive binding assay with ^{68}Ga-labelled PSMA-HBED-CC (PSMA-DKFZ-11) according to the literature with minor modifications [61]. Briefly, each compound at different concentrations (0 – 5000 nM) was incubated for 1 h at 37 °C with 0.15 nM [^{68}Ga]Ga-PSMA-HBED-CC together with 2×10^5 LNCaP cells per well. After incubation, cells were washed three times with ice-cold PBS and cell-associated

activity recovered by addition of 1 M NaOH. Radioactivity was measured by a gamma counter and data fitted using non-linear regression (GraphPad Prism). Experiments were performed two times in triplicate.

2.9. Small-animal PET imaging

All animal experiments complied with the current laws of the Federal Republic of Germany and were conducted according to German Animal welfare guidelines. Normal female athymic Balb/c nude mice (17–20 g, 4–6 weeks old) were obtained from Janvier SAS (St. Berthevin Cedex, France). Mice were provided with food and water *ad libitum*. LNCaP tumors were induced on the shoulder by sub-cutaneous injection of 5×10^6 cells in a 100 µL cell suspension of a 1:1 v/v mixture of media with reconstituted basement membrane (GFR BD Matrigel™, Corning BV, Amsterdam, Holland). After an average of 4 weeks, tumor size reached ~200 – 300 mg and the animals were used for PET imaging studies.

For PET imaging studies, mice were injected with 100 µL sterile filtered phosphate buffered saline formulations pH 7.4 of [^{64}Cu]**4** (6–8 MBq) or [^{68}Ga]**4** (18–23 MBq) by intravenous tail-vein injection and anesthetized with isoflurane (2–4% in air). PET Imaging was performed on a Focus 120 microPET scanner at 30 min, 1 h, 2 h and 3 h post-injection (p.i.). For copper-64, additional scans at 24 h p.i. were performed. Data were acquired for 10, 15 or 60 min in list mode. Reconstruction was performed using unweighted OSEM2D. Image analysis was performed using AMIDE. Image counts per second per voxel (cps/voxel) were calibrated to activity concentrations (Bq mL^{-1}) by measuring a 3.5 cm cylinder phantom filled with a known concentration of radioactivity. Time-activity curves (TACs) were constructed by manually drawing regions of interest (ROI) in the tumor, liver and the kidneys. All ROIs were then copied on each of the frames, and time-activity curves of the ROI mean values were generated.

Competitive inhibition (blocking) studies were also performed *in vivo* and measured using static PET imaging to investigate the specificity of the radiotracers for PSMA. As a blocking agent, non-radiolabelled 2-(phosphonomethyl)pentane-1,5-dioic acid (PMPA; 20 nmol mouse^{-1}) was co-injected with the radiotracers (n = 3) [62].

2.10. Ex vivo biodistribution

For each compound, a total of five animals were injected with [^{64}Cu]**4** (6–8 MBq) or [^{68}Ga]**4** (18–23 MBq) in 100 µL sterile filtered phosphate buffered saline via a tail vein. At 60 min p.i., animals were sacrificed by isoflurane anesthesia. Organs of interest were dissected, weighed and assayed for radioactivity in a gamma counter. The percent injected activity per gram (%IA g^{-1}) for each tissue was calculated by comparison of the tissue counts to a standard sample prepared from the injection solution. Specificity of the radiotracers for PSMA was determined by co-injection of PMPA (20 nmol mouse^{-1}) [62].

3. Results and discussion

3.1. Bioconjugate synthesis

Our previously described triply substituted ligands lack a functionality for the covalent conjugation of biologically active targeting vectors [57]. For this reason, we developed the BFC NODIA-Me **1**, in which we replaced one methylimidazole arm with an acetic acid group (Scheme 2) [58]. This acetic acid group serves as site for the attachment of appropriate targeting vectors via peptide bond formation. The glutamate-urea-lysine (Glu-NH-CO-NH-Lys) structural motif is a well-known building block for the development of potent PSMA inhibitors [63-64]. Besides interactions of the urea and the carboxylic groups with the Zn^{2+} active site of the PSMA binding pocket, there are also lipophilic interactions with an accessible hydrophobic pocket [63, 65]. Therefore, a lipophilic naphthyl-alanine spacer was

introduced via standard Fmoc chemistry to the commercially available precursor Glu-NH-CO-NH-Lys(Ahx)-tBu_3 ester to obtain the intermediate **2** in 97% yield (Scheme 2). Conjugation of NODIA-Me **1** was accomplished using HATU as coupling reagent to give compound **3** in 70% yield. Cleavage of the tBu-esters was accomplished by reaction of **3** in 5 M hydrochloric acid for 16 h to give the final PSMA-bioconjugate **4** in 61% overall yield. The identity and purity of compound **4** (>98%) was determined by NMR spectroscopy, mass spectrometry and analytical RP-HPLC. Corresponding data are given in the Supporting Information.

3.2. Radiochemistry

Radiosynthesis of [^{64}Cu]**4** was accomplished by mixing the bioconjugate **4** with the appropriate radioactivity amount of [^{64}Cu]$CuCl_2$ in ammonium acetate (pH 8.2) followed by incubation for 15 min at ambient temperatures. These mild conditions concur with the results obtained in previous ^{64}Cu-labelling experiments of our ligands bearing three azaheterocyclic arms [57]. The RCP and the decay corrected RCY for [^{64}Cu]**4** were both determined to be >98%.

Radiosynthesis of [^{68}Ga]**4** was performed in an automated, GMP-compliant process by heating compound **4** with [^{68}Ga]$GaCl_3$(aq.) at 95 °C for 10 min [58]. The RCP and the decay corrected RCY for [^{68}Ga]**4** were measured to >98% and for both radiometals molar activities of ~20 MBq $nmol^{-1}$ were obtained.

3.3. Lipophilicity

The log $D_{oct/PBS}$ values of [^{68}Ga]**4** and [^{64}Cu]**4** were measured in an octanol-phosphate buffered saline system (Table 1). Compounds are highly hydrophilic with log $D_{oct/PBS}$ values of -4.27 ± 0.08 and -3.99 ± 0.05 for [^{68}Ga]**4** and [^{64}Cu]**4**, respectively. The order of

lipophilicity was corroborated chromatographically by RP-HPLC (Table 1). The lipophilicity of both compounds is comparable to [^{68}Ga]Ga-PSMA-HBED-CC with log $D_{oct/PBS}$ = -4.06 ± 0.10.

We recently showed that the remaining coordination site of the gallium NODIA-Me complex can be occupied by monodentate ligands such as hydroxide or chloride [58]. The NODIA-Me complex charge can thus be estimated to +2 for [^{68}Ga]**4** and [^{64}Cu]**4**. The deprotonated carboxylic acid functions of the Glu-NH-CO-NH-Lys PSMA-binding motif provide a 3-fold negative charge resulting in an estimated overall charge of both [^{68}Ga]**4** and [^{64}Cu]**4** of -1. In contrast, the PSMA-targeting reference ligand [^{68}Ga]Ga-PSMA-HBED-CC possesses an estimated overall charge of -5 (-1 for the hexadentate N_2O_4-complex to Ga(III) with two carboxylates and two phenolates of the HBED-CC, -1 for the free terminal carboxyethyl-group of HBED-CC, and -3 for deprotonated carboxylic acid functions of the Glu-NH-CO-NH-Lys PSMA-binding motif) [66-68]. Despite the lower overall charge of [^{68}Ga]**4** and [^{64}Cu]**4** at physiological pH, the total number of charges is comparable to [^{68}Ga]Ga-PSMA-HBED-CC. Furthermore, the positively charged NODIA-Me metal chelates result in a zwitterionic nature of the [^{68}Ga]**4** and [^{64}Cu]**4** PSMA-targeting probes.

3.4. In vitro studies

3.4.1. Serum stability studies

The stability of [^{68}Ga]**4** and [^{64}Cu]**4** was assessed *in vitro* by incubation at 37°C in human serum. For [^{68}Ga]**4**, the amount of intact compound decreased from 94 ± 2% at 1 h to 85 ± 3% after 4 h incubation time. The major metabolite of [^{68}Ga]**4** eluted after the dead volume of the system, consistent with the retention time of "free" gallium-68 and/or [^{68}Ga]**1**. The ^{64}Cu-labelled conjugate [^{64}Cu]**4** was found to be more stable with 92 ± 2% intact tracer after 24 h

incubation. The protein associated fractions of [^{68}Ga]**4** and [^{64}Cu]**4** in the serum stability studies were determined to 48 ± 5% and 29 ± 2%, respectively. The protein bound fractions of [^{68}Ga]**4** and [^{64}Cu]**4** compare well to that of [^{68}Ga]Ga-PSMA-HBED-CC, which was determined to 35 ± 3%. Finally, exchange of monodentate ligands such as chloride or hydroxide coordinated to the metal center, as reported previously, was not observed for [^{68}Ga]**4** [58].

3.4.2. Competitive binding assay

The binding affinities of **4**, Ga-**4** and Cu-**4** were determined in a competitive binding assay on LNCaP cells using [^{68}Ga]Ga-PSMA-HBED-CC as radioligand, which yielded IC_{50}-values of 233 ± 10 nM, 176 ± 10 nM and 681 ± 7 nM (Table 1). The IC_{50}-values were converted to K_i-values using the Cheng-Prusoff equation [69] and the reported K_d value for [^{68}Ga]Ga-PSMA-HBED-CC of 2.9 ± 0.6 nM [55]. With K_i values of 222 nM, 167 nM, and 648 nM, respectively, the NODIA-Me based PSMA-targeting ligands **4**, Ga-**4**, and Cu-**4** revealed substantially lower PSMA-binding affinities than [^{68}Ga]Ga-PSMA-HBED-CC. Clearly, the size and charge of the metal chelating unit as well differences in the linker region have a major impact on the PSMA-binding affinity of the whole construct.

Different from HBED-CC, the BFC NODIA-Me **1** does not possess any charge compensating donor groups and, consequently, forms metal complexes with Cu^{2+} and Ga^{3+} that have a positive overall charge. Under physiological conditions, the compounds [^{68}Ga]**4** and [^{64}Cu]**4** presumably possess an estimated overall charge of -1. Even if no metal cation is coordinated to **4**, the NODIA-Me chelating moiety is partially protonated at physiologic pH as the pK_a values for the TACN amino groups are 7.0 and 11.3 and the pK_a value of imidazole is 7.0 [70]. This partial protonation of the metal binding moiety of uncomplexed **4** at physiological pH seems to translate to a PSMA binding affinity comparable to Ga-**4**.

Even though other factors cannot be excluded such as differences in the competition assay (different radioligand), the rather large charge difference between our NODIA-Me based PSMA-targeting probes and [^{68}Ga]Ga-PSMA-HBED-CC may be the primary reason for their lower affinity. Indeed, recent studies by Babich and coworkers on ^{99m}Tc(CO$_3$)-labeled PSMA inhibitors containing functionalized imidazole rings have shown that charge has a major impact on binding affinity [71-72]. In a series of probes based on the Glu-NH-CO-NH-Lys PSMA-binding motif and single amino acid chelate (SAAC) systems containing substituted di-imidazoles, increasing derivatization of the imidazole rings with negatively charged carboxylic acid functional groups resulted in significantly improved affinity for PSMA [71]. Building on these findings, addition of carboxylate groups to our NODIA-Me chelating platform may pave the way to a second generation of PSMA-targeting probes with higher affinity.

Interestingly, however, the PSMA binding affinity of [^{64}Cu]**4** is almost 4-times lower than that of [^{68}Ga]**4** (both potentially having an overall charge of -1), suggesting that binding affinity of the probes is not a simple function of complex charge, but instead results from an interplay of several factors. Similar to our findings, the ^{64}Cu-complex of the recently reported PSMA-targeting probe (R)-NODAGA-Phe-Phe-D-Lys(suberoyl)-Lys-urea-Glu (CC34) showed a higher K_d-value than its ^{68}Ga-labeled counterpart [55].

3.5. In vivo studies

The aim of this study was to demonstrate the radiochemical scope and utility of the BFC NODIA-Me **1** for radiopharmaceutical design. Therefore, the stability and pharmacokinetic profiles of the ^{68}Ga- and ^{64}Cu-labelled PSMA conjugate **4** were assessed *in vivo*. The distribution and targeting of [^{68}Ga]**4** and [^{64}Cu]**4** in mice bearing subcutaneous PSMA-

positive LNCaP tumors was measured by small-animal PET imaging and *ex vivo* biodistribution studies.

3.5.1. Small-animal PET imaging

The pharmacokinetics of [^{68}Ga]**4** and [^{64}Cu]**4** were assessed by small-animal PET imaging of nude mice bearing LNCaP xenografts at 30 min, 1, 2 and 3 h post injection (p.i.) as well as after 24 h for [^{64}Cu]**4**. Corresponding maximum intensity projections (MIPs) for [^{68}Ga]**4** and [^{64}Cu]**4** at 1 h p.i. are given in Figure 1. In addition, volume-of-interest (VOI) analysis was performed for both compounds on the LNCaP tumor, liver and kidneys (Figure 2).

The distribution of radiotracers differs from each other with [^{64}Cu]**4** exhibiting a slightly higher uptake than [^{68}Ga]**4** in the majority of organs, which is potentially a consequence of its higher lipophilicity compared to [^{68}Ga]**4** (Table 1). Overall, uptake of both compounds in background organs was low due to their rapid blood pool clearance and renal excretion. Both conjugates [^{68}Ga]**4** and [^{64}Cu]**4** showed specific accumulation in PSMA positive LNCaP tumors (Figure 2A+C). Tumor uptake peaked at 30 min p.i. with 0.92% and 1.53% injected activity per gram (% IA g^{-1}) for [^{68}Ga]**4** and [^{64}Cu]**4**, respectively. A slow washout from the LNCaP tumors occurred for both compounds declining from 0.75% IA g^{-1} at 1 h p.i. to 0.41% IA g^{-1} at 3 h p.i. for [^{68}Ga]**4**. The conjugate [^{64}Cu]**4** exhibited a slower washout than [^{68}Ga]**4** with 1.14% IA g^{-1} at 1 h p.i. decreasing to 0.88% IA g^{-1} at 3 h p.i. and a prolonged retention with 0.39% IA g^{-1} still present in the tumor after 24 h. Compared to ^{68}Ga-PSMA-HBEC-CC with a tumor uptake of ~3.5% IA g^{-1} at 1 h p.i. in similar PET-imaging studies [46], the tumor uptake of [^{68}Ga]**4** and [^{64}Cu]**4** in our studies at the same time point (1 h p.i.) was lower. However, tumor uptake is known to be dependent on the PSMA expression level of the specific batch of LNCaP-tumors and the total amount of the radioligand injected (~1 nmol of radioligand / mouse in our study), e.g., tumor uptake values in the report of Eder et *al.* [46]

were ~3.5% IA g^{-1} in their PET study (~0.5 nmol / mouse) compared to 7.70 ± 1.45% IA g^{-1} in their *ex vivo* biodistribution study (0.1 – 0.2 nmol / mouse), while others even reported values of 15.8 ± 1.4% IA g^{-1} for an ex vivo biodistribution study with 10 pmol per mouse [55]. Specific uptake of [^{68}Ga]**4** and [^{64}Cu]**4** was demonstrated by blockade of PSMA using co-administration of PMPA. Blocking experiments resulted in a statistically significant reduction of tumor uptake ($P < 0.05$ over all time points) (Figure 2B + D).

Liver uptake was very low for [^{68}Ga]**4** with 0.37% IA g^{-1} at 30 min p.i. reaching essentially background levels at 3 h p.i. (Figure 2A). For [^{64}Cu]**4**, uptake peaked at 30 min p.i. with 1.31% IA g^{-1} and then plateaued at ~0.7–1.0% IA g^{-1} up to 24 h (Figure 2C). At all time points studied, the liver uptake of [^{64}Cu]**4** was slightly higher than that of [^{68}Ga]**4**, which might be attributed to differences in lipophilicity (Table 1) or, alternatively, suggest instability of [^{64}Cu]**4** and superoxide dismutase (SOD1) dependent transchelation [73]. Importantly, however, the liver uptake of about 1.0% IA g^{-1} for [^{64}Cu]**4** is comparable to the liver uptake of the best candidates identified in an extensive study directed towards the development of novel ^{64}Cu-labeled PSMA-inhibitors based on the same lysine-urea-glutamate scaffold, and stability of these probes was considered suitable for clinical translation [12].

Both [^{68}Ga]**4** and [^{64}Cu]**4** exhibited rapid blood pool clearance and renal excretion. Corresponding activity levels in the kidneys declined from 4.39% IA g^{-1} at 30 min p.i. to 0.88% IA g^{-1} after 3 h for [^{68}Ga]**4**, and from 3.31% IA g^{-1} at 30 min p.i. to 1.05% IA g^{-1} after 3 h for [^{64}Cu]**4** (Figure 2A+C). Both compounds showed much lower kidney accumulation and faster washout compared to [^{68}Ga]Ga-PSMA-HBED-CC and [^{68}Ga]Ga-PSMA-617, consistent with their lower affinity for PSMA [46, 56]. In corresponding blocking studies, the kidney uptake was significantly reduced for [^{68}Ga]**4**, whereas only a slight decrease was noted for [^{64}Cu]**4** (Figure 2B+D). Despite the low affinity of both tracers for PSMA, the low

accumulation and retention of [^{68}Ga]**4** and [^{64}Cu]**4** in the kidneys is still noteworthy. In previous PET imaging studies of our ^{64}Cu-labelled trisubstituted chelators (in absence of a targeting vector), we found high uptake in the liver (~11–17% IA g^{-1}) and the kidneys (~20–40% IA g^{-1}) at 1 h p.i. for the imidazole-type ligands, respectively [57]. It remained unclear whether the uptake in liver and kidneys was a result of the positive charge or due to demetallation/transchelation. The data of the current PET imaging study shows that the biodistribution of both radiotracers is mainly determined by the PSMA targeting vector rather than the positive overall charge of the metal chelates and that rapid clearance and low uptake in background organs is consistent with kinetically stable metal chelates.

3.5.2. Ex vivo biodistribution

In addition to the PET imaging studies, we also assayed the pharmacokinetics and the stability of [^{68}Ga]**4** and [^{64}Cu]**4** by *ex vivo* biodistribution studies (Table 2). Corresponding results of selected organs at 1 h p.i. are summarized in Figure 3. In general, results follow the same trend as seen in the PET imaging experiments, however, absolute uptake values obtained from *ex vivo* biodistribution studies were slightly higher than those calculated from the PET imaging data. Uptake of [^{68}Ga]**4** was low in all organs with < 1% IA g^{-1} at 1 h p.i. with exception of the kidneys, which are known to express PSMA [74]. For [^{64}Cu]**4**, low but overall higher accumulation compared to that of [^{68}Ga]**4** was noted in the kidneys, liver, lung and intestine. The kidney uptake for [^{68}Ga]**4** and [^{64}Cu]**4** with 6.28% IA g^{-1} and 4.96% IA g^{-1} was significantly lower than that reported for [^{68}Ga]Ga-PSMA-HBED-CC and [^{68}Ga]Ga-PSMA-617 with 139.4% IA g^{-1} and 113.3% IA g^{-1}, respectively [46, 56, 61]. Accumulation in the kidneys was PSMA-specific and could be reduced by co-injection of PMPA by ~80% and ~72% for [^{68}Ga]**4** and [^{64}Cu]**4**, respectively (Table 2). Liver uptake of [^{64}Cu]**4** was higher than that of [^{68}Ga]**4** but was reduced by almost 50% after co-injection of PMPA. Compared

to [^{68}Ga]Ga-PSMA-HBED-CC (0.87% IA g^{-1}) and [^{68}Ga]Ga-PSMA-617 (1.17% IA g^{-1}) [46, 61], liver accumulation was lower for [^{68}Ga]**4** (0.30% IA g^{-1}), while it was about two-fold higher for [^{64}Cu]**4** (2.69 % IA g^{-1}). Nevertheless, this rather low value is not indicative of complex instability and substantial transchelation *in vivo*.

Tumor accumulation of [^{68}Ga]**4** with 1.33% IA g^{-1} was lower than that of [^{64}Cu]**4** with 2.15% IA g^{-1}. In comparison to [^{68}Ga]Ga-PSMA-HBED-CC and [^{68}Ga]Ga-PSMA-617, which have reported tumor uptake of 7.70 and 8.47% IA g^{-1} [46, 61], respectively, [^{68}Ga]**4** and [^{64}Cu]**4** exhibited lower accumulation in the tumor. This is in line with the lower PSMA binding affinity of our NODIA-Me based PSMA targeting probes compared to [^{68}Ga]Ga-PSMA-HBED-CC and [^{68}Ga]Ga-PSMA-617 [55-56, 61]. A promising strategy for improvement of binding affinity and tumor targeting properties may be the addition of pendant carboxylic acids to the imidazole-groups of the NODIA-Me chelating moiety, as these negatively charged functional groups were reported to lead to additional PSMA binding interactions for a series of similar imidazole-containing PSMA targeting probes (*vide supra*) [71]. PSMA specificity of [^{68}Ga]**4** and [^{64}Cu]**4** was confirmed by co-injection of PMPA resulting in reduction of tumor uptake by ~88% and ~70%, respectively. Interestingly, the relatively low kidney accumulation and retention of [^{68}Ga]**4** and [^{64}Cu]**4** resulted in significantly improved tumor-to-kidney ratios of 0.21 and 0.43, respectively. These values are ~3-8fold higher than those of [^{68}Ga]Ga-PSMA-HBED-CC and [^{68}Ga]Ga-PSMA-617 with 0.055 and 0.074 [46, 56, 61].

4. Conclusions

In the present work, the novel chelator NODIA-Me **1** was conjugated to the PSMA targeting Glu-NH-CO-NH-Lys moiety to give the final bioconjugate **4**, which was labelled with gallium-68 and copper-64 in molar activities of ~20 MBq $nmol^{-1}$. The metal-free as well as the Ga and Cu complexes of **4** revealed different affinities to PSMA in competitive binding studies underscoring the influence of the metal chelate on biological properties. Evaluation of the ^{68}Ga- and ^{64}Cu-labelled conjugates by PET imaging and *ex vivo* biodistribution studies demonstrated PSMA-specific tumor uptake. Both compounds exhibited low kidney uptake, rapid renal clearance, and only low uptake in non-target organs. Liver accumulation was very low for [^{68}Ga]**4**, while it was moderately increased for [^{64}Cu]**4**, which could be either due to the higher lipophilicity of the ^{64}Cu-complex or suggest a very limited level of transchelation. Strategies towards further improvement of binding affinity and tumor targeting of the NODIA-Me based PSMA-binding probes may include introduction of additional negative charges in the chelating unit by functionalization of the imidazoles with pendant carboxylic acid arms and optimization of the spacer moiety. Overall, the results indicate that imidazole-based TACN chelators show promise for the future development of ^{68}Ga- and ^{64}Cu-labelled radiopharmaceuticals.

Acknowledgements

JPH thanks the Department of Nuclear Medicine, University Hospital Freiburg, the German Cancer Consortium (DKTK), and the German Cancer Research Center (DKFZ) for financial support as well as the Swiss National Science Foundation (SNSF Professorship PP00P2_163683) and the European Research Council (ERC-StG-2015, NanoSCAN – 676904). MDB thanks the Chemistry Department of the Albert-Ludwigs-University Freiburg (Germany) for technical support, in particular Christoph Warth for MS measurements, Manfred Keller for NMR measurements and Prof. Philipp Kurz for his continuous support. MDB also thanks the Research Commission of the University Freiburg as well as the Fonds der chemischen Industrie for financial support.

References

[1] Bartholoma, M. D.; Louie, A. S.; Valliant, J. F.; Zubieta, J. Technetium and Gallium Derived Radiopharmaceuticals: Comparing and Contrasting the Chemistry of Two Important Radiometals for the Molecular Imaging Era. Chem Rev 2010; 110: 2903-2920.

[2] Decristoforo, C.; Pickett, R. D.; Verbruggen, A. Feasibility and availability of (6)(8)Ga-labelled peptides. Eur J Nucl Med Mol Imaging 2012; 39 Suppl 1: S31-40.

[3] Breeman, W. A.; de Blois, E.; Sze Chan, H.; Konijnenberg, M.; Kwekkeboom, D. J.; Krenning, E. P. (68)Ga-labeled DOTA-peptides and (68)Ga-labeled radiopharmaceuticals for positron emission tomography: current status of research, clinical applications, and future perspectives. Semin Nucl Med 2011; 41: 314-321.

[4] Fani, M.; Andre, J. P.; Maecke, H. R. 68Ga-PET: a powerful generator-based alternative to cyclotron-based PET radiopharmaceuticals. Contrast Media Mol Imaging 2008; 3: 67-77.

[5] Velikyan, I. 68Ga-Based radiopharmaceuticals: production and application relationship. Molecules 2015; 20: 12913-12943.

[6] Bartholomä, M. D. Recent developments in the design of bifunctional chelators for metal-based radiopharmaceuticals used in Positron Emission Tomography. Inorg Chim Acta 2012; 389: 36-51.

[7] Wadas, T. J.; Wong, E. H.; Weisman, G. R.; Anderson, C. J. Copper chelation chemistry and its role in copper radiopharmaceuticals. Curr Pharm Des 2007; 13: 3-16.

[8] Ikotun, O. F.; Lapi, S. E. The rise of metal radionuclides in medical imaging: copper-64, zirconium-89 and yttrium-86. Future Med Chem 2011; 3: 599-621.

[9] Blower, P. J.; Lewis, J. S.; Zweit, J. Copper radionuclides and radiopharmaceuticals in nuclear medicine. Nucl Med Biol 1996; 23: 957-980.

[10] Dumont, R. A.; Tamma, M.; Braun, F.; Borkowski, S.; Reubi, J. C.; Maecke, H., et al. Targeted Radiotherapy of Prostate Cancer with a Gastrin-Releasing Peptide Receptor Antagonist Is Effective as Monotherapy and in Combination with Rapamycin. J Nucl Med 2013; 54: 762-769.

[11] Dumont, R. A.; Deininger, F.; Haubner, R.; Maecke, H. R.; Weber, W. A.; Fani, M. Novel Cu-64- and Ga-68-Labeled RGD Conjugates Show Improved PET Imaging of alpha(v)beta(3) Integrin Expression and Facile Radiosynthesis. J Nucl Med 2011; 52: 1276-1284.

[12] Banerjee, S. R.; Pullambhatla, M.; Foss, C. A.; Nimmagadda, S.; Ferdani, R.; Anderson, C. J., et al. 64Cu-Labeled Inhibitors of Prostate-Specific Membrane Antigen for PET Imaging of Prostate Cancer. J Med Chem 2014; 57: 2657-2669.

[13] Dearling, J. L.; Paterson, B. M.; Akurathi, V.; Betanzos-Lara, S.; Treves, S. T.; Voss, S. D., et al. The ionic charge of copper-64 complexes conjugated to an engineered antibody affects biodistribution. Bioconjug Chem 2015; 26: 707-717.

[14] Dearling, J. L.; Voss, S. D.; Dunning, P.; Snay, E.; Fahey, F.; Smith, S. V., et al. Imaging cancer using PET--the effect of the bifunctional chelator on the biodistribution of a (64)Cu-labeled antibody. Nucl Med Biol 2011; 38: 29-38.

[15] Liu, Z.; Yan, Y.; Liu, S.; Wang, F.; Chen, X. 18F, 64Cu, and 68Ga Labeled RGD-Bombesin Heterodimeric Peptides for PET Imaging of Breast Cancer. Bioconjugate Chem 2009; 20: 1016-1025.

[16] Li, Z.-B.; Chen, K.; Chen, X. 68Ga-labeled multimeric RGD peptides for microPET imaging of integrin αvβ3 expression. Eur J Nucl Med Mol Imaging 2008; 35: 1100-1108.

[17] Velikyan, I.; Maecke, H.; Langstrom, B. Convenient Preparation of 68Ga-Based PET-Radiopharmaceuticals at Room Temperature. Bioconjugate Chem 2008; 19: 569-573.
[18] Jeong, J. M.; Hong, M. K.; Chang, Y. S.; Lee, Y.-S.; Kim, Y. J.; Cheon, G. J., et al. Preparation of a Promising Angiogenesis PET Imaging Agent: 68Ga-Labeled c(RGDyK)–Isothiocyanatobenzyl-1,4,7-Triazacyclononane-1,4,7-Triacetic Acid and Feasibility Studies in Mice. J Nucl Med 2008; 49: 830-836.
[19] Ait-Mohand, S.; Fournier, P.; Dumulon-Perreault, V.; Kiefer, G. E.; Jurek, P.; Ferreira, C. L., et al. Evaluation of 64Cu-labeled bifunctional chelate-bombesin conjugates. Bioconjug Chem 2011; 22: 1729-1735.
[20] Lane, S. R.; Nanda, P.; Rold, T. L.; Sieckman, G. L.; Figueroa, S. D.; Hoffman, T. J., et al. Optimization, biological evaluation and microPET imaging of copper-64-labeled bombesin agonists, [64Cu-NO2A-(X)-BBN(7-14)NH2], in a prostate tumor xenografted mouse model. Nucl Med Biol 2010; 37: 751-761.
[21] Wieser, G.; Mansi, R.; Grosu, A. L.; Schultze-Seemann, W.; Dumont-Walter, R. A.; Meyer, P. T., et al. Positron emission tomography (PET) imaging of prostate cancer with a gastrin releasing peptide receptor antagonist--from mice to men. Theranostics 2014; 4: 412-419.
[22] Notni, J.; Hermann, P.; Havlickova, J.; Kotek, J.; Kubicek, V.; Plutnar, J., et al. A triazacyclononane-based bifunctional phosphinate ligand for the preparation of multimeric 68Ga tracers for positron emission tomography. Chem Eur J 2010; 16: 7174-7185.
[23] Notni, J.; Šimeček, J.; Hermann, P.; Wester, H.-J. TRAP, a Powerful and Versatile Framework for Gallium-68 Radiopharmaceuticals. Chem Eur J 2011; 17: 14718-14722.
[24] Notni, J.; Pohle, K.; Wester, H. J. Be spoilt for choice with radiolabelled RGD peptides: preclinical evaluation of (6)(8)Ga-TRAP(RGD)(3). Nucl Med Biol 2013; 40: 33-41.
[25] Ferreira, C. L.; Lamsa, E.; Woods, M.; Duan, Y.; Fernando, P.; Bensimon, C., et al. Evaluation of Bifunctional Chelates for the Development of Gallium-Based Radiopharmaceuticals. Bioconjugate Chem 2010; 21: 531-536.
[26] Tircsó, G.; Benyó, E. T.; Suh, E. H.; Jurek, P.; Kiefer, G. E.; Sherry, A. D., et al. (S)-5-(p-Nitrobenzyl)-PCTA, a Promising Bifunctional Ligand with Advantageous Metal Ion Complexation Kinetics. Bioconjugate Chem 2009; 20: 565-575.
[27] Ferreira, C. L.; Yapp, D. T. T.; Mandel, D.; Gill, R. K.; Boros, E.; Wong, M. Q., et al. 68Ga Small Peptide Imaging: Comparison of NOTA and PCTA. Bioconjugate Chem 2012; 23: 2239-2246.
[28] Boal, A. K.; Rosenzweig, A. C. Structural biology of copper trafficking. Chem Rev 2009; 109: 4760-4779.
[29] Cai, H.; Fissekis, J.; Conti, P. S. Synthesis of a novel bifunctional chelator AmBaSar based on sarcophagine for peptide conjugation and (64)Cu radiolabelling. Dalton Trans 2009, 10.1039/b902210d [doi] 5395-5400.
[30] Cai, H.; Li, Z.; Huang, C. W.; Park, R.; Shahinian, A. H.; Conti, P. S. An improved synthesis and biological evaluation of a new cage-like bifunctional chelator, 4-((8-amino-3,6,10,13,16,19-hexaazabicyclo[6.6.6]icosane-1-ylamino)methyl)benzoic acid, for 64Cu radiopharmaceuticals. Nucl Med Biol 2010; 37: 57-65.
[31] Di Bartolo, N.; Sargeson, A. M.; Smith, S. V. New 64Cu PET imaging agents for personalised medicine and drug development using the hexa-aza cage, SarAr. Org Biomol Chem 2006; 4: 3350-3357.
[32] Di Bartolo, N. M.; Sargeson, A. M.; Donlevy, T. M.; Smith, S. V. Synthesis of a new cage ligand, SarAr, and its complexation with selected transition metal ions for potential use in radioimaging. J Chem Soc, Dalton Trans 2001, 10.1039/b103242a 2303-2309.

[33] Boswell, C. A.; Sun, X.; Niu, W.; Weisman, G. R.; Wong, E. H.; Rheingold, A. L., et al. Comparative in vivo stability of copper-64-labeled cross-bridged and conventional tetraazamacrocyclic complexes. J Med Chem 2004; 47: 1465-1474.
[34] Garrison, J. C.; Rold, T. L.; Sieckman, G. L.; Figueroa, S. D.; Volkert, W. A.; Jurisson, S. S., et al. In vivo evaluation and small-animal PET/CT of a prostate cancer mouse model using 64Cu bombesin analogs: side-by-side comparison of the CB-TE2A and DOTA chelation systems. J Nucl Med 2007; 48: 1327-1337.
[35] Hausner, S. H.; Kukis, D. L.; Gagnon, M. K.; Stanecki, C. E.; Ferdani, R.; Marshall, J. F., et al. Evaluation of [64Cu]Cu-DOTA and [64Cu]Cu-CB-TE2A chelates for targeted positron emission tomography with an alphavbeta6-specific peptide. Mol Imaging 2009; 8: 111-121.
[36] Sprague, J. E.; Peng, Y.; Fiamengo, A. L.; Woodin, K. S.; Southwick, E. A.; Weisman, G. R., et al. Synthesis, Characterization and In Vivo Studies of Cu(II)-64-Labeled Cross-Bridged Tetraazamacrocycle-amide Complexes as Models of Peptide Conjugate Imaging Agents. J Med Chem 2007; 50: 2527-2535.
[37] Sun, X.; Wuest, M.; Weisman, G. R.; Wong, E. H.; Reed, D. P.; Boswell, C. A., et al. Radiolabeling and in vivo behavior of copper-64-labeled cross-bridged cyclam ligands. J Med Chem 2002; 45: 469-477.
[38] Wadas, T. J.; Anderson, C. J. Radiolabeling of TETA- and CB-TE2A-conjugated peptides with copper-64. Nat Protoc 2006; 1: 3062-3068.
[39] Juran, S.; Walther, M.; Stephan, H.; Bergmann, R.; Steinbach, J.; Kraus, W., et al. Hexadentate bispidine derivatives as versatile bifunctional chelate agents for copper(II) radioisotopes. Bioconjug Chem 2009; 20: 347-359.
[40] Stephan, H.; Walther, M.; Fahnemann, S.; Ceroni, P.; Molloy, J. K.; Bergamini, G., et al. Bispidines for dual imaging. Chemistry (Easton) 2014; 20: 17011-17018.
[41] Comba, P.; Hunoldt, S.; Morgen, M.; Pietzsch, J.; Stephan, H.; Wadepohl, H. Optimization of pentadentate bispidines as bifunctional chelators for 64Cu positron emission tomography (PET). Inorg Chem 2013; 52: 8131-8143.
[42] Cai, Z. X.; Anderson, C. J. Chelators for copper radionuclides in positron emission tomography radiopharmaceuticals. J Labelled Compd Radiopharm 2014; 57: 224-230.
[43] Spang, P.; Herrmann, C.; Roesch, F. Bifunctional Gallium-68 Chelators: Past, Present, and Future. Seminars in Nuclear Medicine 2016; 46: 373-394.
[44] Zeglis, B. M.; Houghton, J. L.; Evans, M. J.; Viola-Villegas, N.; Lewis, J. S. Underscoring the Influence of Inorganic Chemistry on Nuclear Imaging with Radiometals. Inorg Chem 2014; 53: 1880-1899.
[45] Holland, J. P.; Williamson, M. J.; Lewis, J. S. Unconventional Nuclides for Radiopharmaceuticals. Molecular Imaging 2010; 9: 1-20.
[46] Eder, M.; Schäfer, M.; Bauder-Wüst, U.; Hull, W.-E.; Wängler, C.; Mier, W., et al. 68Ga-Complex Lipophilicity and the Targeting Property of a Urea-Based PSMA Inhibitor for PET Imaging. Bioconjugate Chem 2012; 23: 688-697.
[47] Israeli, R. S.; Powell, C. T.; Fair, W. R.; Heston, W. D. Molecular cloning of a complementary DNA encoding a prostate-specific membrane antigen. Cancer Res 1993; 53: 227-230.
[48] Horoszewicz, J. S.; Kawinski, E.; Murphy, G. P. Monoclonal antibodies to a new antigenic marker in epithelial prostatic cells and serum of prostatic cancer patients. Anticancer Res 1987; 7: 927-935.
[49] Rong, S. B.; Zhang, J.; Neale, J. H.; Wroblewski, J. T.; Wang, S.; Kozikowski, A. P. Molecular modeling of the interactions of glutamate carboxypeptidase II with its potent NAAG-based inhibitors. J Med Chem 2002; 45: 4140-4152.

[50] Zhang, A. X.; Murelli, R. P.; Barinka, C.; Michel, J.; Cocleaza, A.; Jorgensen, W. L., et al. A remote arene-binding site on prostate specific membrane antigen revealed by antibody-recruiting small molecules. J Am Chem Soc 2010; 132: 12711-12716.
[51] Eder, M.; Neels, O.; Muller, M.; Bauder-Wust, U.; Remde, Y.; Schafer, M., et al. Novel Preclinical and Radiopharmaceutical Aspects of [68Ga]Ga-PSMA-HBED-CC: A New PET Tracer for Imaging of Prostate Cancer. Pharmaceuticals (Basel) 2014; 7: 779-796.
[52] Weineisen, M.; Schottelius, M.; Simecek, J.; Baum, R. P.; Yildiz, A.; Beykan, S., et al. 68Ga- and 177Lu-Labeled PSMA I&T: Optimization of a PSMA-Targeted Theranostic Concept and First Proof-of-Concept Human Studies. J Nucl Med 2015; 56: 1169-1176.
[53] Herrmann, K.; Bluemel, C.; Weineisen, M.; Schottelius, M.; Wester, H.-J.; Czernin, J., et al. Biodistribution and Radiation Dosimetry for a Probe Targeting Prostate-Specific Membrane Antigen for Imaging and Therapy. J Nucl Med 2015; 56: 855-861.
[54] Chatalic, K. L.; Heskamp, S.; Konijnenberg, M.; Molkenboer-Kuenen, J. D.; Franssen, G. M.; Clahsen-van Groningen, M. C., et al. Towards Personalized Treatment of Prostate Cancer: PSMA I&T, a Promising Prostate-Specific Membrane Antigen-Targeted Theranostic Agent. Theranostics 2016; 6: 849-861.
[55] Gourni, E.; Canovas, C.; Goncalves, V.; Denat, F.; Meyer, P. T.; Maecke, H. R. (R)-NODAGA-PSMA: A Versatile Precursor for Radiometal Labeling and Nuclear Imaging of PSMA-Positive Tumors. PLoS One 2015; 10: e0145755.
[56] Benešová, M.; Schäfer, M.; Bauder-Wüst, U.; Afshar-Oromieh, A.; Kratochwil, C.; Mier, W., et al. Preclinical Evaluation of a Tailor-Made DOTA-Conjugated PSMA Inhibitor with Optimized Linker Moiety for Imaging and Endoradiotherapy of Prostate Cancer. J Nucl Med 2015; 56: 914-920.
[57] Gotzmann, C.; Braun, F.; Bartholomä, M. D. Synthesis, 64Cu-labeling and PET imaging of 1,4,7-triazacyclononane derived chelators with pendant azaheterocyclic arms. RSC Advances 2016; 6: 119-131.
[58] Schmidtke, A.; Läppchen, T.; Weinmann, C.; Bier-Schorr, L.; Keller, M.; Kiefer, Y., et al. Gallium Complexation, Stability, and Bioconjugation of 1,4,7-Triazacyclononane Derived Chelators with Azaheterocyclic Arms. Inorg Chem 2017, 10.1021/acs.inorgchem.7b01129.
[59] Jilg, C. A.; Drendel, V.; Rischke, H. C.; Beck, T.; Vach, W.; Schaal, K., et al. Diagnostic Accuracy of Ga-68-HBED-CC-PSMA-Ligand-PET/CT before Salvage Lymph Node Dissection for Recurrent Prostate Cancer. Theranostics 2017; 7: 1770-1780.
[60] Zanzonico, P. Routine quality controlof clinical nucliear medicine instrumentation: a brief review. J Nucl Med 2009; 49: 1114-1131.
[61] Benešová, M.; Bauder-Wüst, U.; Schäfer, M.; Klika, K. D.; Mier, W.; Haberkorn, U., et al. Linker Modification Strategies To Control the Prostate-Specific Membrane Antigen (PSMA)-Targeting and Pharmacokinetic Properties of DOTA-Conjugated PSMA Inhibitors. J Med Chem 2016; 59: 1761-1775.
[62] Kratochwil, C.; Giesel, F. L.; Leotta, K.; Eder, M.; Hoppe-Tich, T.; Youssoufian, H., et al. PMPA for Nephroprotection in PSMA-Targeted Radionuclide Therapy of Prostate Cancer. J Nucl Med 2015; 56: 293-298.
[63] Barinka, C.; Byun, Y.; Dusich, C. L.; Banerjee, S. R.; Chen, Y.; Castanares, M., et al. Interactions between human glutamate carboxypeptidase II and urea-based inhibitors: structural characterization. J Med Chem 2008; 51: 7737-7743.
[64] Banerjee, S. R.; Pullambhatla, M.; Shallal, H.; Lisok, A.; Mease, R. C.; Pomper, M. G. A modular strategy to prepare multivalent inhibitors of prostate-specific membrane antigen (PSMA). Oncotarget 2011; 2: 1244-1253.

[65] Mesters, J. R.; Barinka, C.; Li, W.; Tsukamoto, T.; Majer, P.; Slusher, B. S., et al. Structure of glutamate carboxypeptidase II, a drug target in neuronal damage and prostate cancer. EMBO J 2006; 25: 1375-1384.
[66] Zoller, M.; Schuhmacher, J.; Reed, J.; Maierborst, W.; Matzku, S. Establishment and Characterization of Monoclonal-Antibodies against an Octahedral Gallium Chelate Suitable for Immunoscintigraphy with Pet. J Nucl Med 1992; 33: 1366-1372.
[67] Leplatte.F; Murase, I.; Martell, A. E. New Multidentate Ligands .6. Chelating Tendencies of N,N'-Di(2-Hydroxybenzyl) Ethylenediamine-N,N'-Diacetic Acid. J Am Chem Soc 1967; 89: 837-&.
[68] Banerjee, S. R.; Chen, Z. P.; Pullambhatla, M.; Lisok, A.; Chen, J.; Mease, R. C., et al. Preclinical Comparative Study of Ga-68-Labeled DOTA, NOTA, and HBED-CC Chelated Radiotracers for Targeting PSMA. Bioconjugate Chem 2016; 27: 1447-1455.
[69] Cheng, Y.; Prusoff, W. H. Relationship between Inhibition Constant (K1) and Concentration of Inhibitor Which Causes 50 Per Cent Inhibition (I50) of an Enzymatic-Reaction. Biochem Pharmacol 1973; 22: 3099-3108.
[70] Vandermerwe, M. J.; Boeyens, J. C. A.; Hancock, R. D. Crystallographic and Thermodynamic Study of Metal-Ion Size Selectivity in the Ligand 1,4,7-Triazacyclononane-N,N',N''-Triacetate. Inorg Chem 1985; 24: 1208-1213.
[71] Maresca, K. P.; Hillier, S. M.; Lu, G. L.; Marquis, J. C.; Zimmerman, C. N.; Eckelman, W. C., et al. Small molecule inhibitors of PSMA incorporating technetium-99m for imaging prostate cancer: Effects of chelate design on pharmacokinetics. Inorg Chim Acta 2012; 389: 168-175.
[72] Hillier, S. M.; Maresca, K. P.; Lu, G. L.; Merkin, R. D.; Marquis, J. C.; Zimmerman, C. N., et al. Tc-99m-Labeled Small-Molecule Inhibitors of Prostate-Specific Membrane Antigen for Molecular Imaging of Prostate Cancer. J Nucl Med 2013; 54: 1369-1376.
[73] Zarschler, K.; Kubeil, M.; Stephan, H. Establishment of two complementary in vitro assays for radiocopper complexes achieving reliable and comparable evaluation of in vivo stability. RSC Advances 2014; 4: 10157-10164.
[74] Silver, D. A.; Pellicer, I.; Fair, W. R.; Heston, W. D. W.; CordonCardo, C. Prostate-specific membrane antigen expression in normal and malignant human tissues. Clinical Cancer Research 1997; 3: 81-85.

Figure and Scheme Legends

Scheme 1. Selected chelators for copper-64 and gallium-68.

Scheme 2. Synthesis of PSMA targeting conjugate **4**. i) HATU, DIPEA, DMF, r.t., 70%; ii) 5 M HCl, r.t., 91%.

Figure 1. Representative maximum intensity projections (MIPs) of (A) [^{68}Ga]**4** and (C) [^{64}Cu]**4** at 1 h p.i. in LNCaP tumor bearing mice. Blocking studies confirmed the specificity of (B) [^{68}Ga]**4** and (D) [^{64}Cu]**4** for PSMA expression. White arrows indicate organs of interest: T = tumor, K = kidney, L = liver.

Figure 2. Bar diagram of the volume-of-interest (VOI) analysis for (A) [^{68}Ga]**4** and (C) [^{64}Cu]**4** in the tumor, the liver, and the kidneys from 30 min – 3 h post administration. Corresponding VOI analysis after co-injection of PSMA blocking agent (PMPA) for (B) [^{68}Ga]**4** and (D) [^{64}Cu]**4**. For [^{64}Cu]**4**, data is also provided for 24 h p.i. Legend applies for charts A-D.

Figure 3. *Ex vivo* biodistribution of [^{68}Ga]**4** and [^{64}Cu]**4** for selected organs in LNCaP tumor bearing mice at 1 h p.i along with blocking studies. Data are expressed as %IA g^{-1} and represent mean ± SD (n = 5).

Table 1. Analytical data of prepared compounds.

Compound	Mass calc.	Mass found	$HPLC_{UV/vis}$ t_R [min]	$HPLC_{rad}$ t_R [min] [d)]	Log $D_{oct/PBS}$	IC_{50} [nM]
[$^{nat/68}$Ga]**4**	1053.4432[a)]	1053.4426	15:33	15:50	-4.27 ± 0.08	176 ± 10
[$^{nat/64}$Cu]**4**	1048.4550[b)]	1048.4551	17:42	17:43	-3.99 ± 0.05	681 ± 7

a) $[M - 2H]^+ = [C_{49}H_{68}N_{12}O_{10}Ga]^+$, b) $[M - H]^+ = [C_{49}H_{69}N_{12}O_{10}Cu]^+$, UV/vis and radioactivity detector in series.

Table 2. *Ex vivo* biodistribution of [^{68}Ga]**4** and [^{64}Cu]**4** in mice bearing PSMA-positive LNCaP tumors at 1 h p.i along with blocking studies. Data are expressed as %IA g^{-1} and represent mean ± SD (n = 5).

	[^{68}Ga]-**4**		[^{64}Cu]-**4**	
	1 h	**1 h blockade**	**1 h**	**1 h blockade**
blood	0.37 ± 0.15	0.31 ± 0.16	0.31 ± 0.07	0.16 ± 0.01
heart	0.17 ± 0.06	0.15 ± 0.08	0.45 ± 0.09	0.27 ± 0.04
lung	0.50 ± 0.13	0.29 ± 0.08	1.22 ± 0.56	0.49 ± 0.07
spleen	0.46 ± 0.44	0.13 ± 0.04	0.49 ± 0.05	0.21 ± 0.05
liver	0.30 ± 0.22	0.19 ± 0.02	2.69 ± 0.64	1.48 ± 0.27
pancreas	0.17 ± 0.10	0.11 ± 0.05	0.26 ± 0.01	0.14 ± 0.03
stomach	0.30 ± 0.39	0.13 ± 0.08	0.49 ± 0.22	0.25 ± 0.19
intestine	0.34 ± 0.20	0.20 ± 0.15	1.05 ± 0.10	0.83 ± 0.35
kidney	6.28 ± 0.92	1.25 ± 0.23	4.96 ± 0.79	1.39 ± 0.05
muscle	0.16 ± 0.16	0.14 ± 0.11	0.19 ± 0.01	0.62 ± 0.39
bone	0.21 ± 0.23	0.14 ± 0.04	0.19 ± 0.03	0.33 ± 0.28
tumor	1.33 ± 0.46	0.17 ± 0.13	2.15 ± 0.38	0.65 ± 0.04
tumor:blood	3.59		6.32	
tumor:kidney	0.21		0.43	
tumor:liver	4.43		0.80	

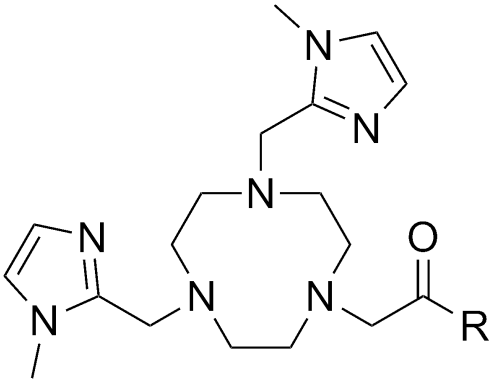

NODIA-Me (R = OH)
conjugated NODIA-Me (R = NH-vector)

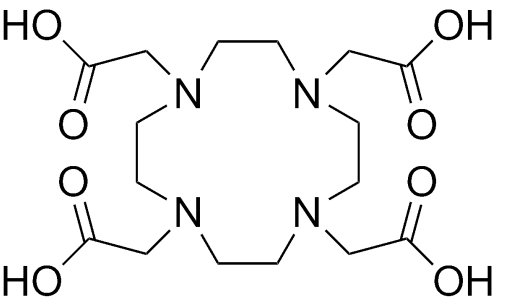

DOTA

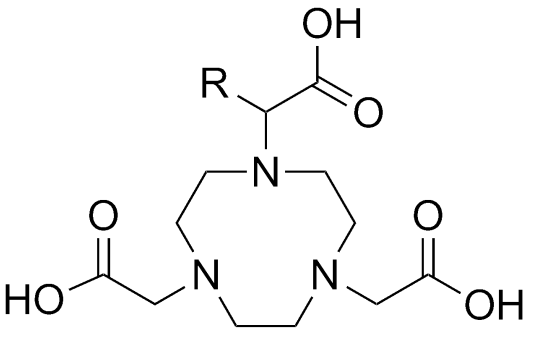

NOTA (R = H)
NODAGA (R = -$(CH_2)_2$-COOH)

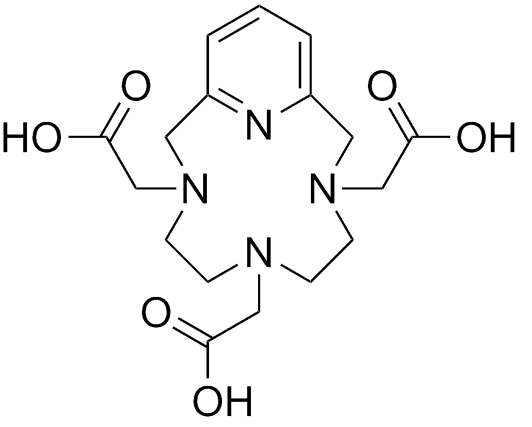

PCTA

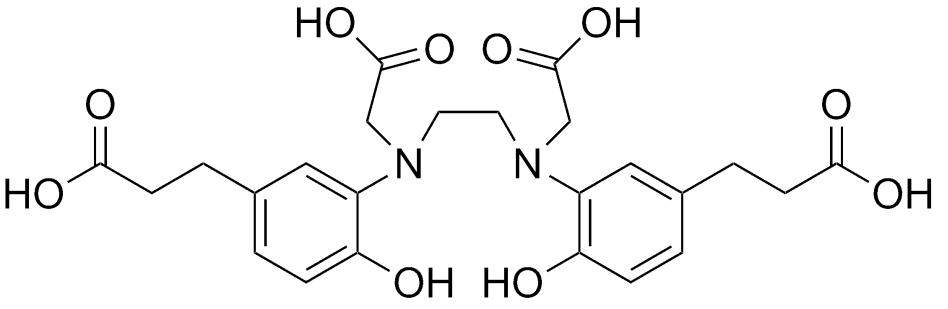

HBED-CC

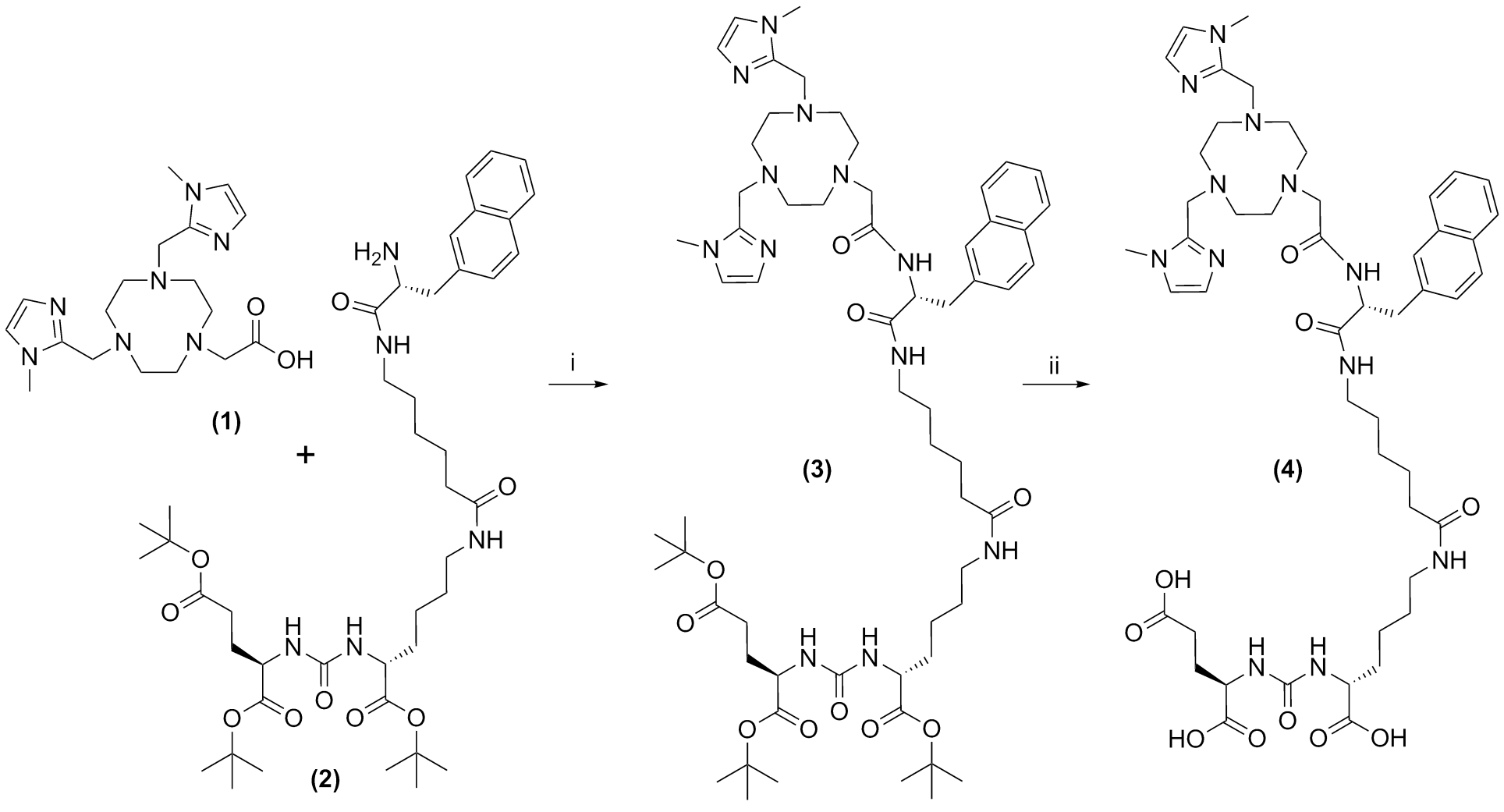
(1)
+
(2)
i
(3)
ii
(4)

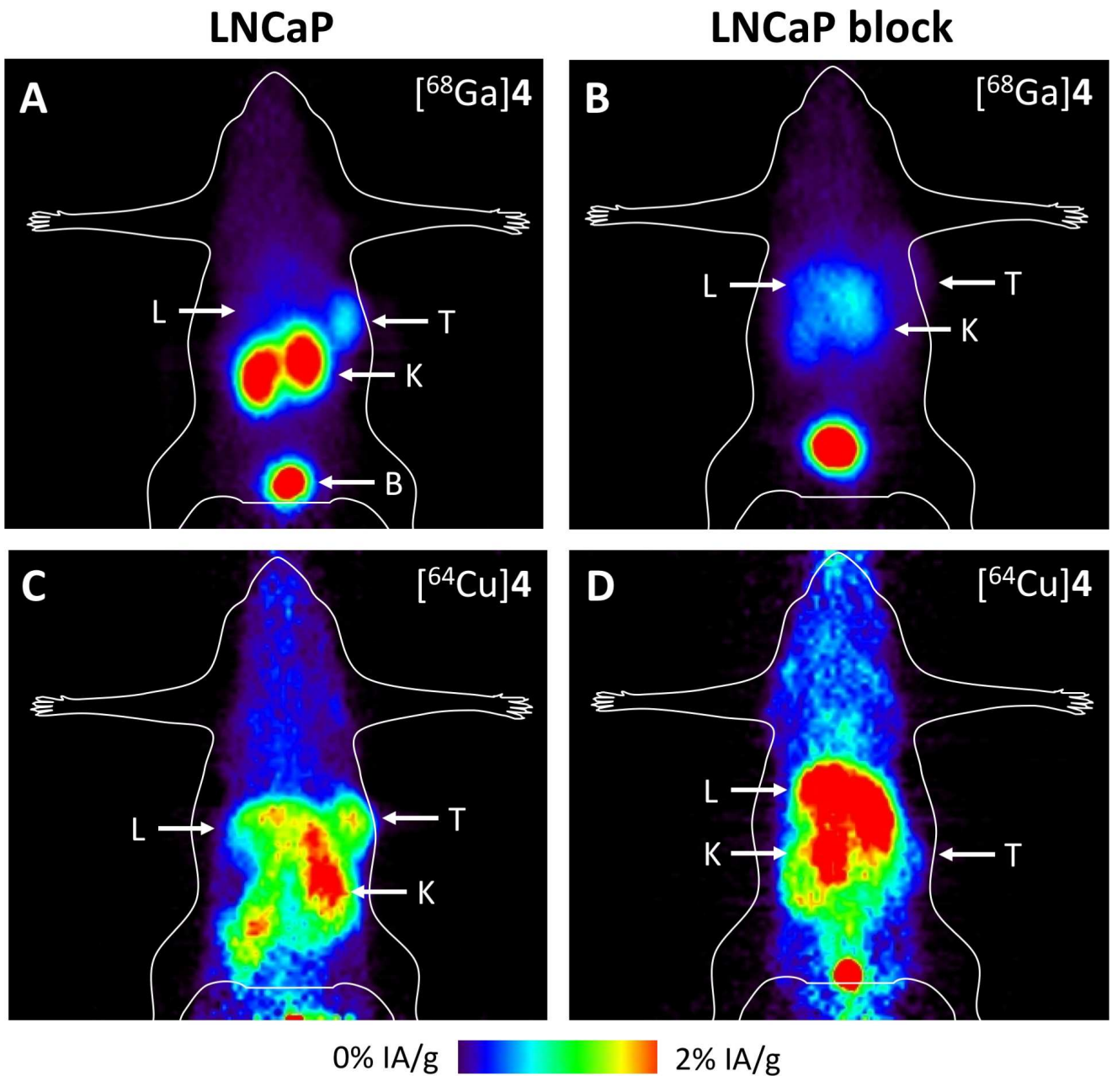
LNCaP
LNCaP block
A
[68Ga]4
L
T
K
B
B
[68Ga]4
L
T
K
C
[64Cu]4
L
T
K
D
[64Cu]4
L
K
T
0% IA/g
2% IA/g

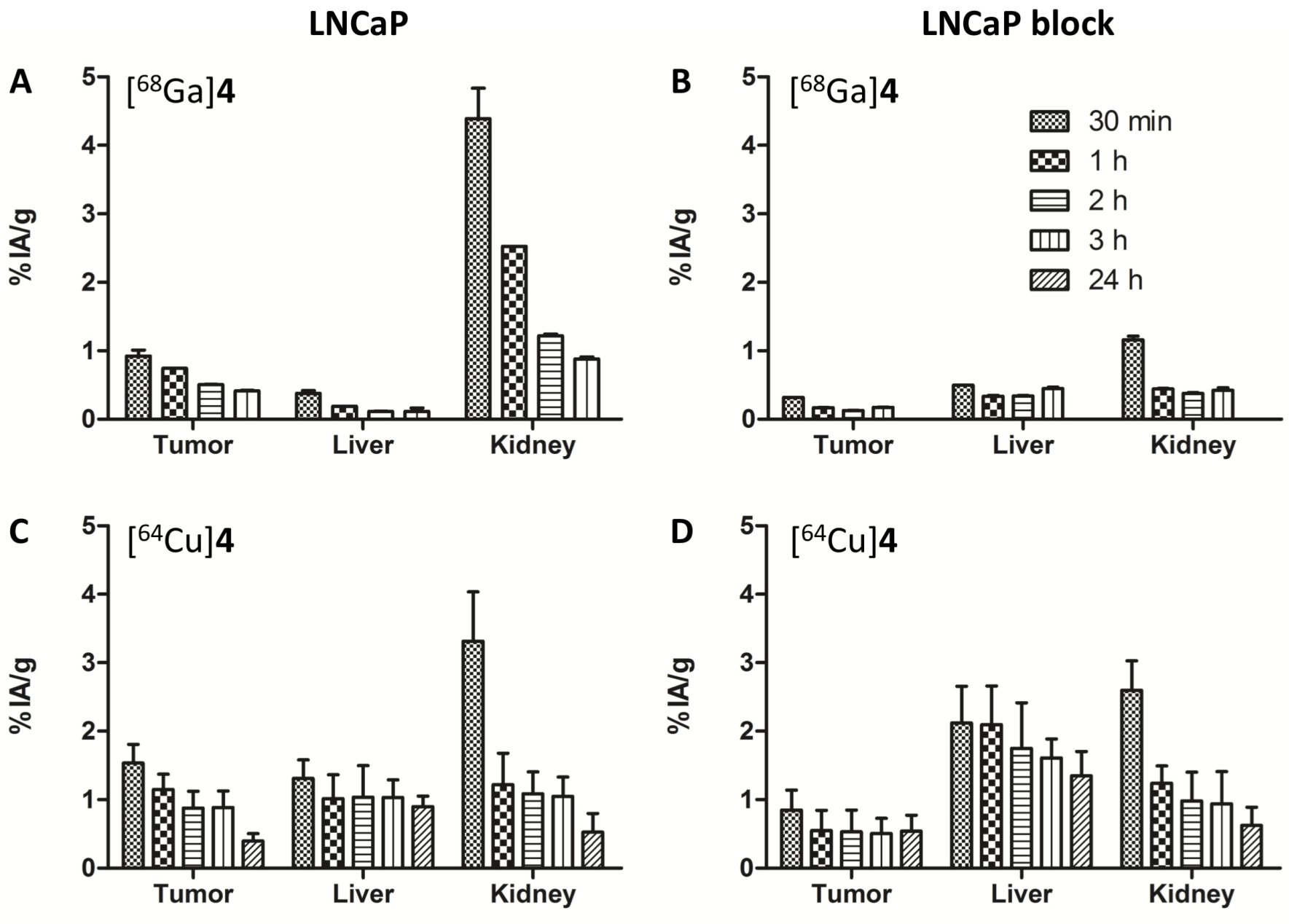
LNCaP
LNCaP block
A
B
C
D
[68Ga]4
[64Cu]4
%IA/g
0
1
2
3
4
5
Tumor
Liver
Kidney
30 min
1 h
2 h
3 h
24 h

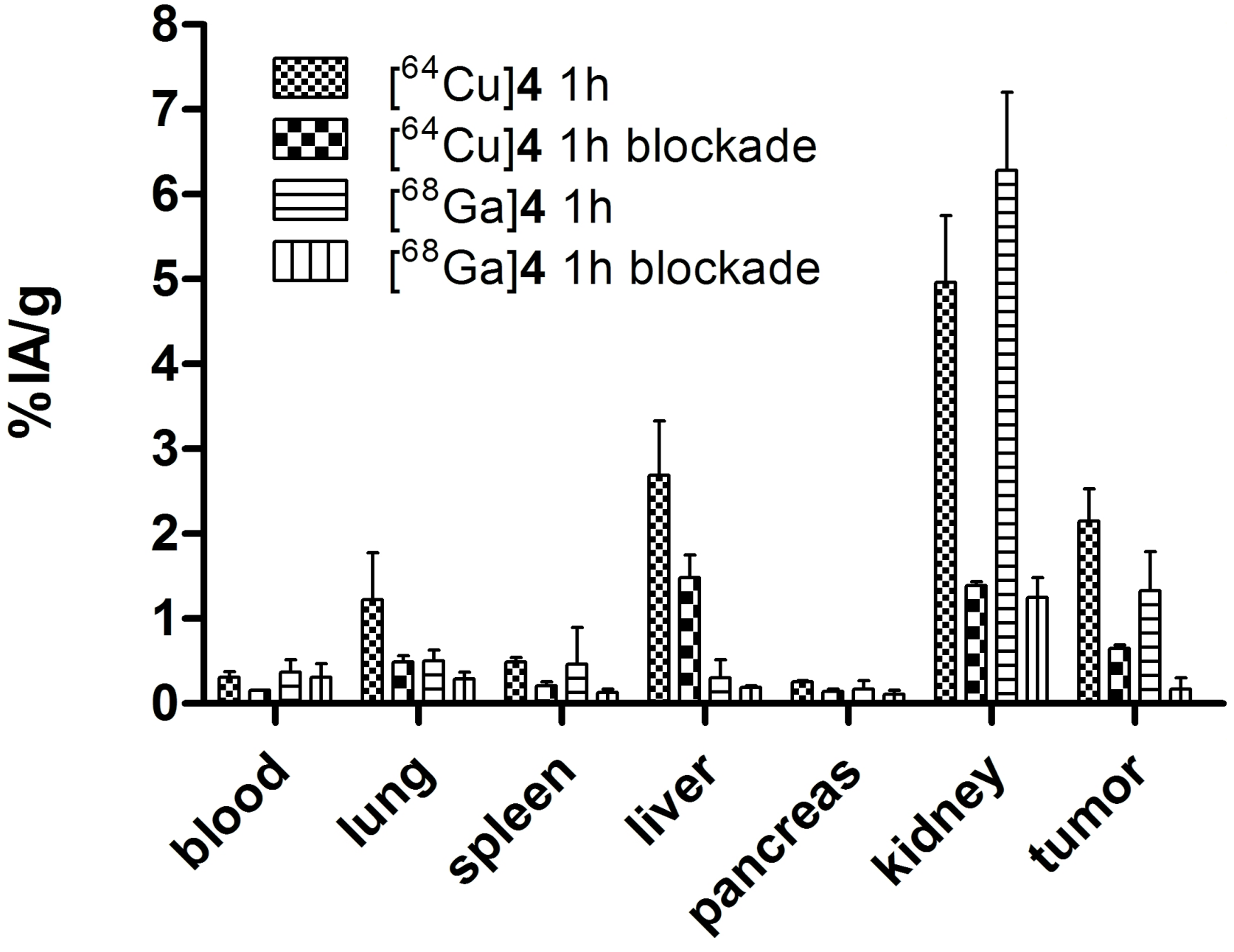
%IA/g
8
7
6
5
4
3
2
1
0
[64Cu]4 1h
[64Cu]4 1h blockade
[68Ga]4 1h
[68Ga]4 1h blockade
blood
lung
spleen
liver
pancreas
kidney
tumor

SUPPORTING INFORMATION

In vitro and in vivo evaluation of the bifunctional chelator NODIA-Me in combination with a prostate-specific membrane antigen targeting vector

Tilman Läppchen[1,2], Yvonne Kiefer[1], Jason P. Holland[1,3], and Mark D. Bartholomä[1,*]

[1] Department of Nuclear Medicine, Medical Center – University of Freiburg, Faculty of Medicine, University of Freiburg, Hugstetterstrasse 55, D-79106, Freiburg, Germany

[2] Department of Nuclear Medicine, Inselspital, Bern University Hospital and University of Bern, Freiburgstrasse, CH-3010 Bern, Switzerland

[3] Department of Chemistry, University of Zürich, Winterthurerstrasse 190, CH-8057, Zürich, Switzerland

*** Corresponding Author:**

Dr. Mark D. Bartholomä

Tel: +49-(761)-270-39600

Fax: +49-(761)-270-39300

E-mail: mark.bartholomae@uniklinik-freiburg.de

Content

NMR characterization

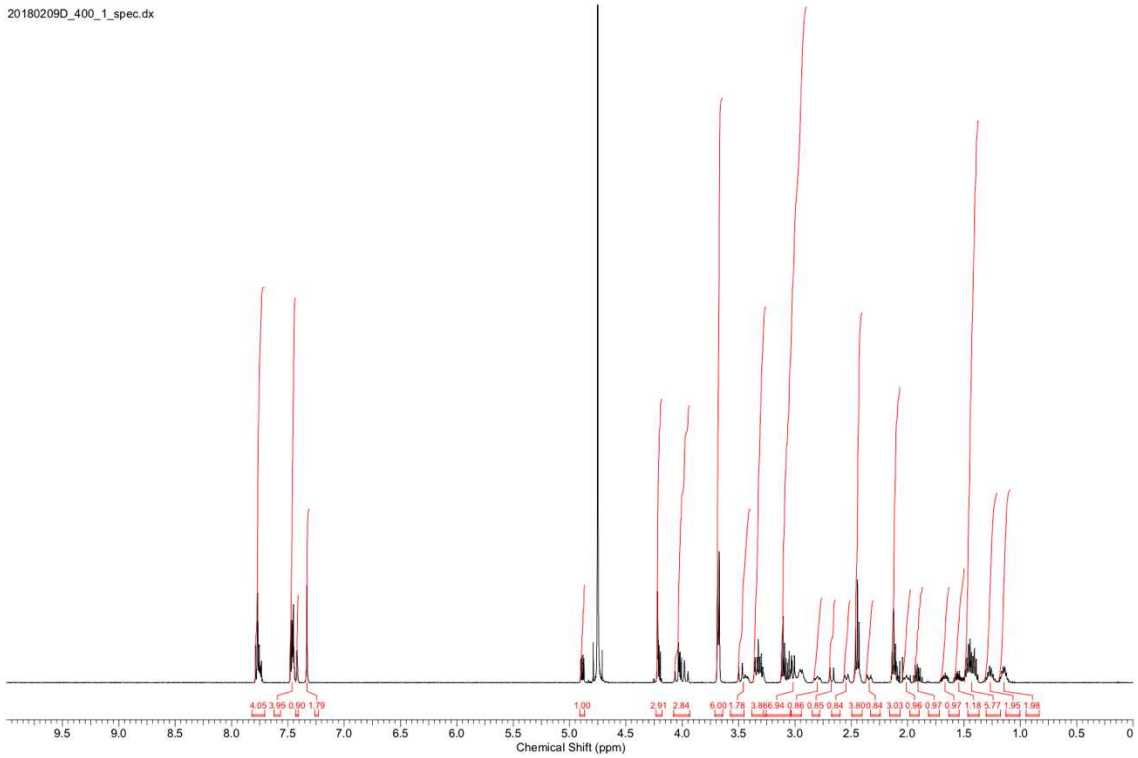

Figure S1. ^{1}H-NMR spectrum of compound **4** in D_2O (pD ≤ 2).

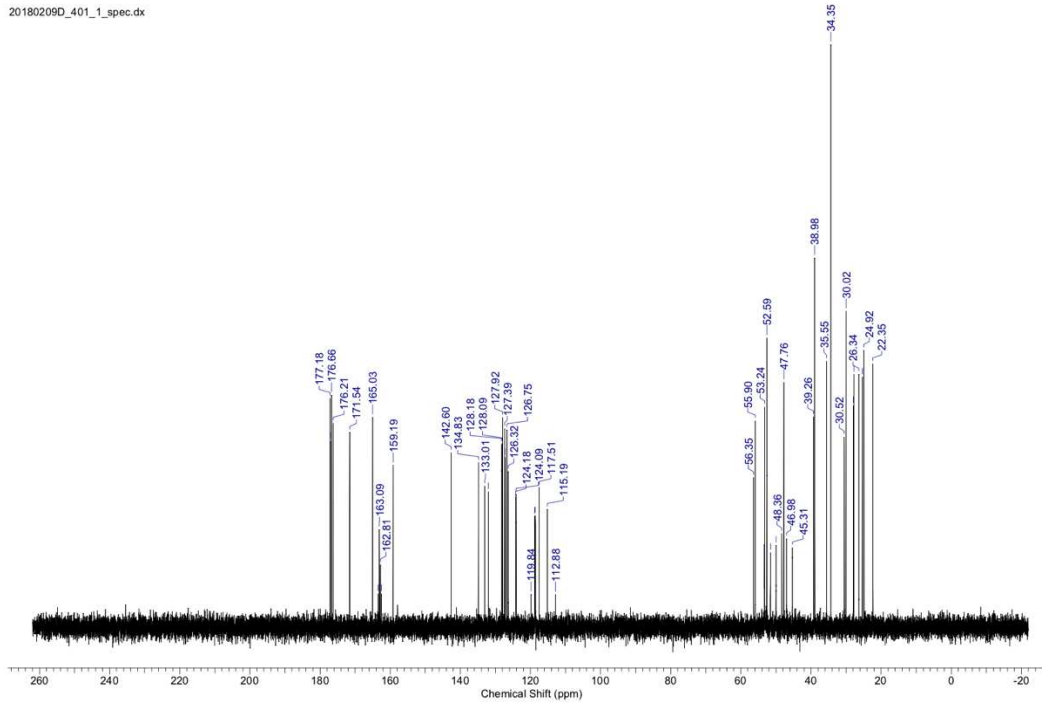

Figure S2. 13C-NMR of compound **4** in D_2O (pD ≤ 2)

Mass spectrometry

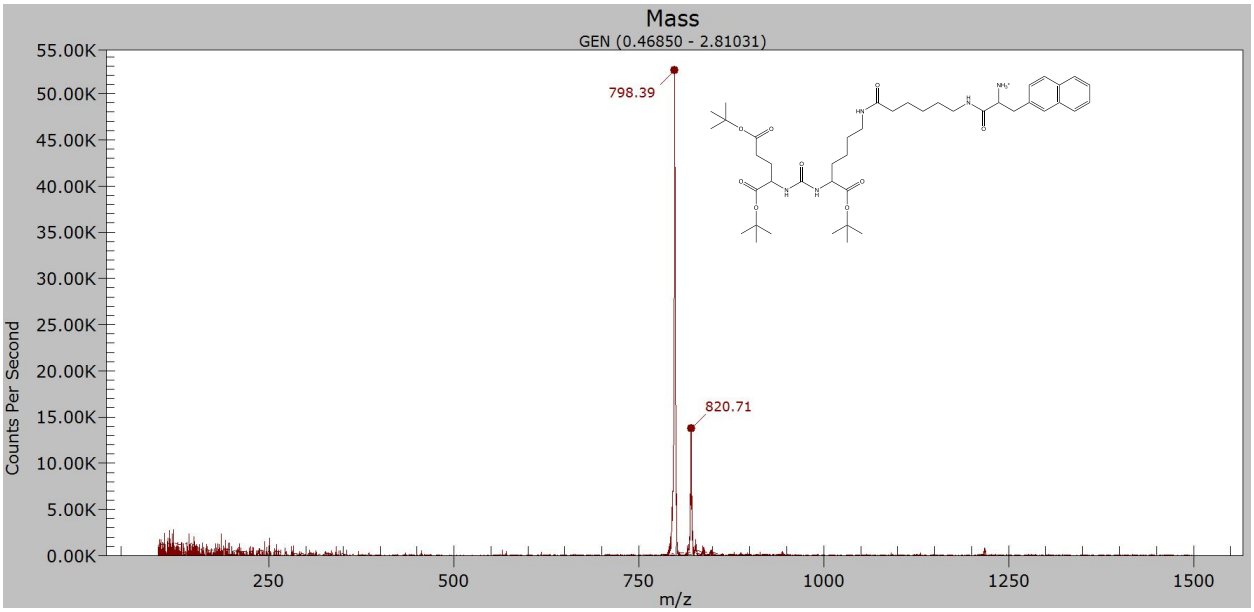

Figure S3. LR-ESI(+)-mass spectrum of **2**.

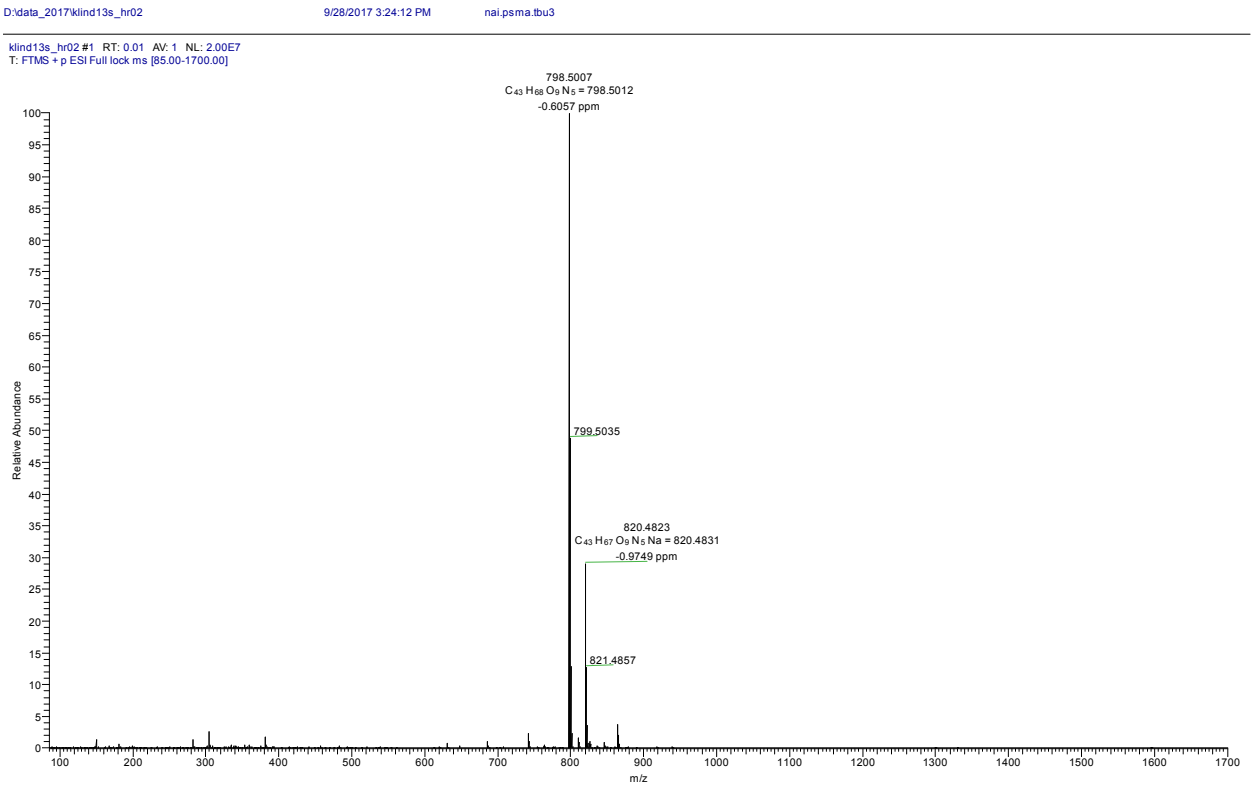

Figure S4. HR-ESI(+)-mass spectrum of **2**. Calc. for $[M+H]^+ = [C_{43}H_{68}N_5O_9]^+ = 798.5012$.

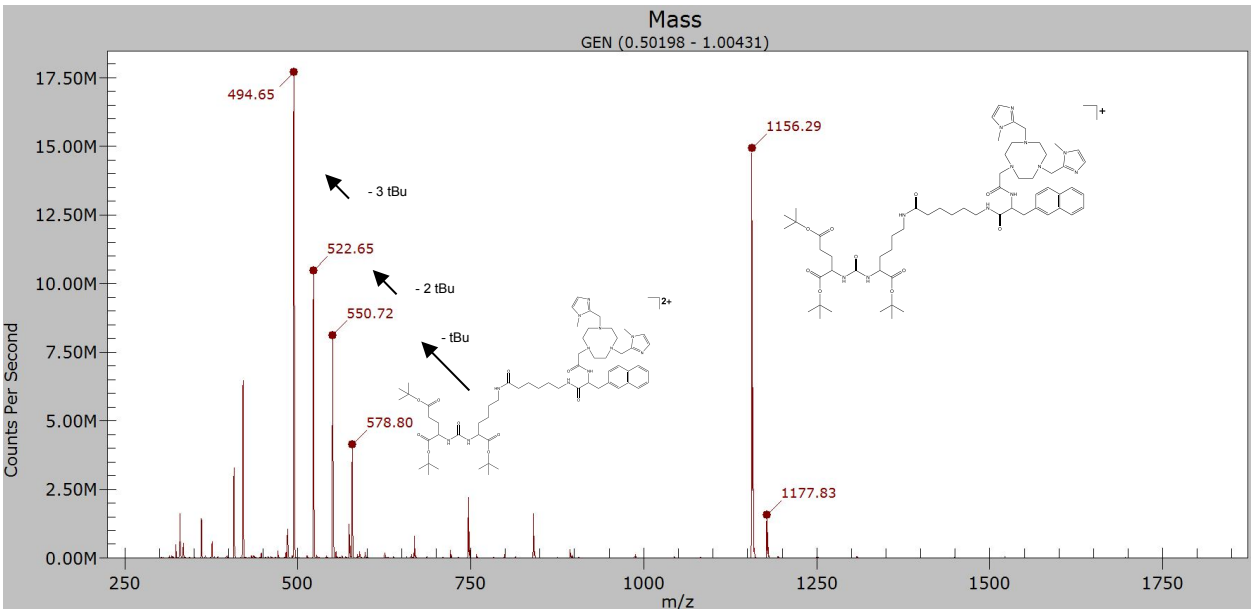

Figure S5. LR-ESI(+)-mass spectrum of **3**.

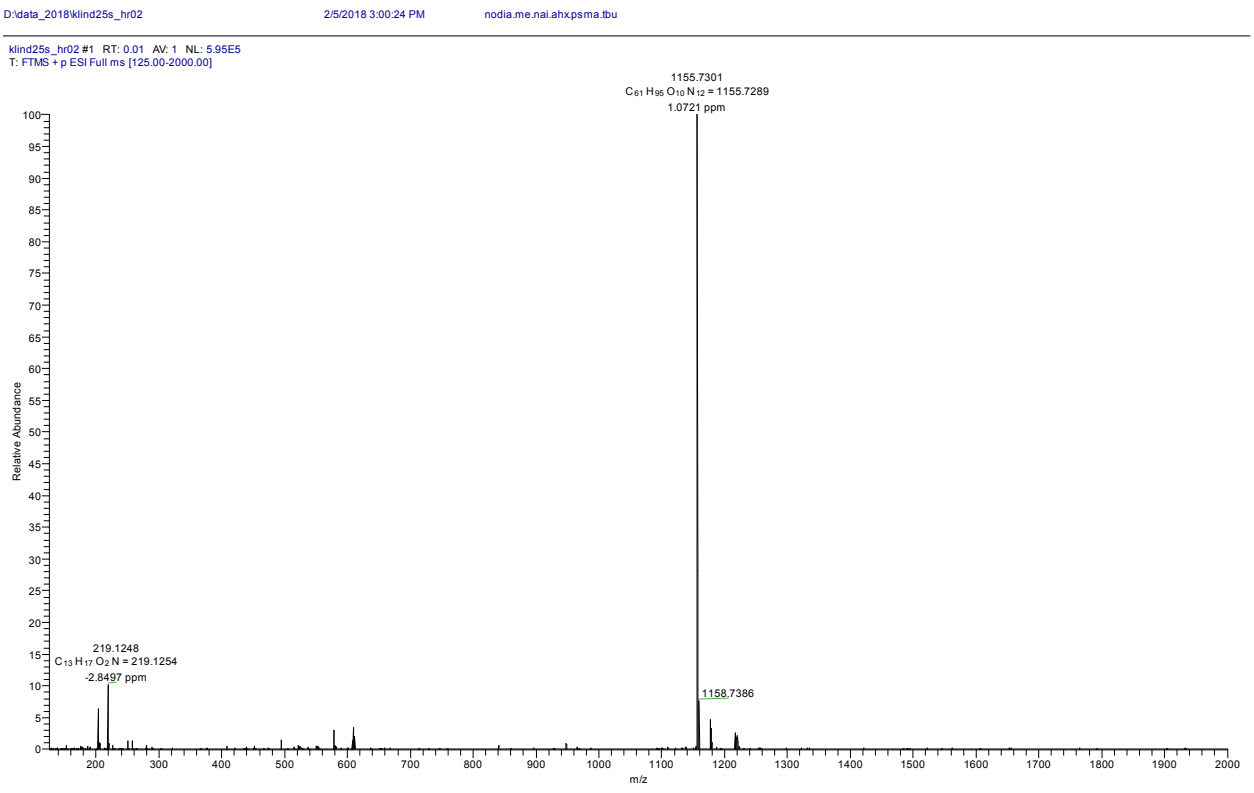

Figure S6. HR-ESI(+)-mass spectrum of **3**. Calc. for $[M+H]^+ = [C_{61}H_{95}N_{12}O_{10}]^+ = 1155.7289$.

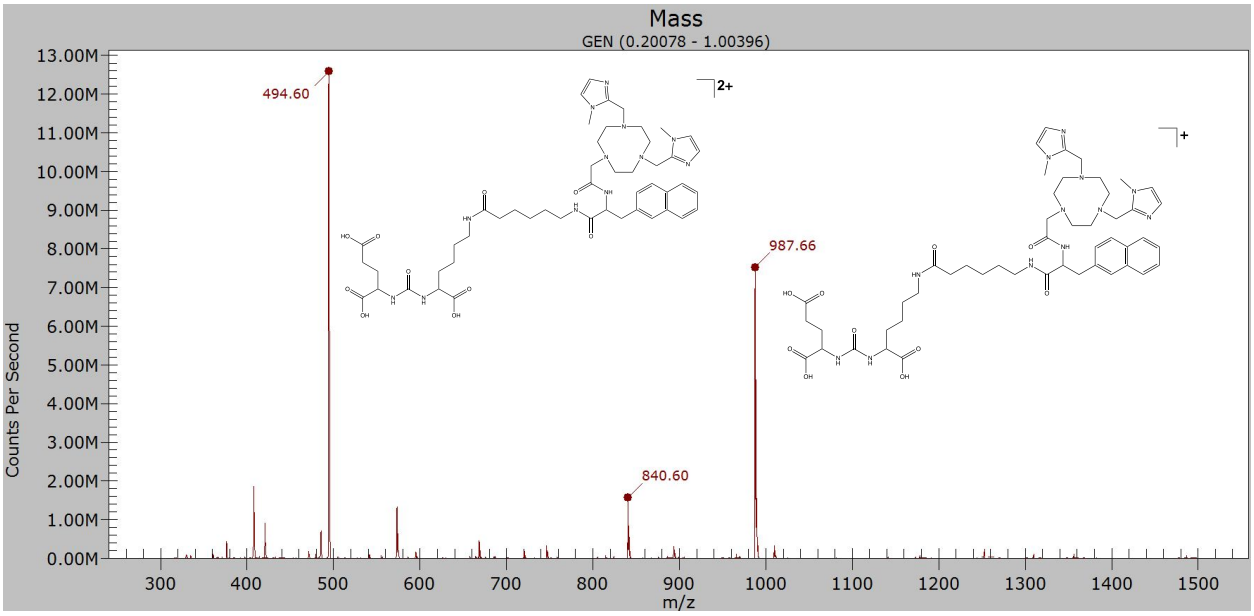

Figure S7. LR-ESI(+)-mass spectrum of **4**.

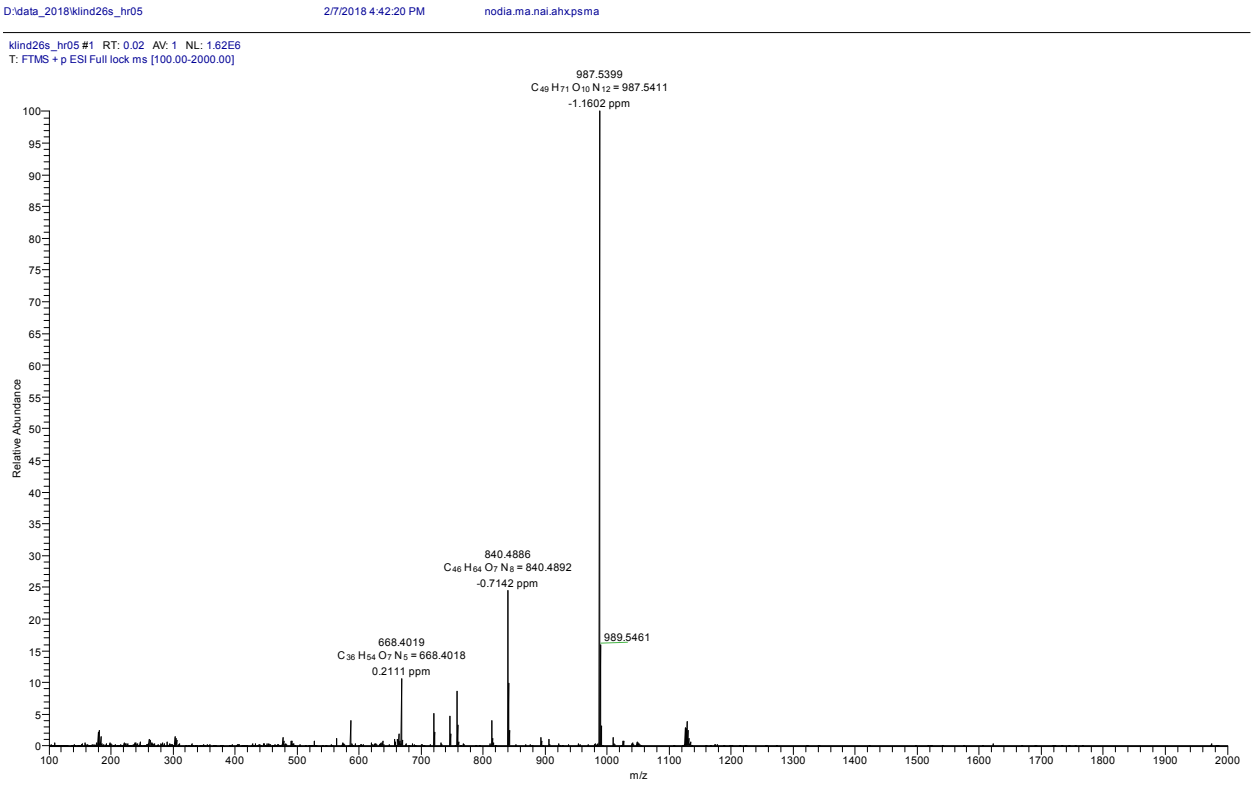

Figure S8. HR-ESI(+)-mass spectrum of **4**. Calc. for $[M+H]^+ = [C_{49}H_{71}N_{12}O_{10}]^+ = 987.5411$.

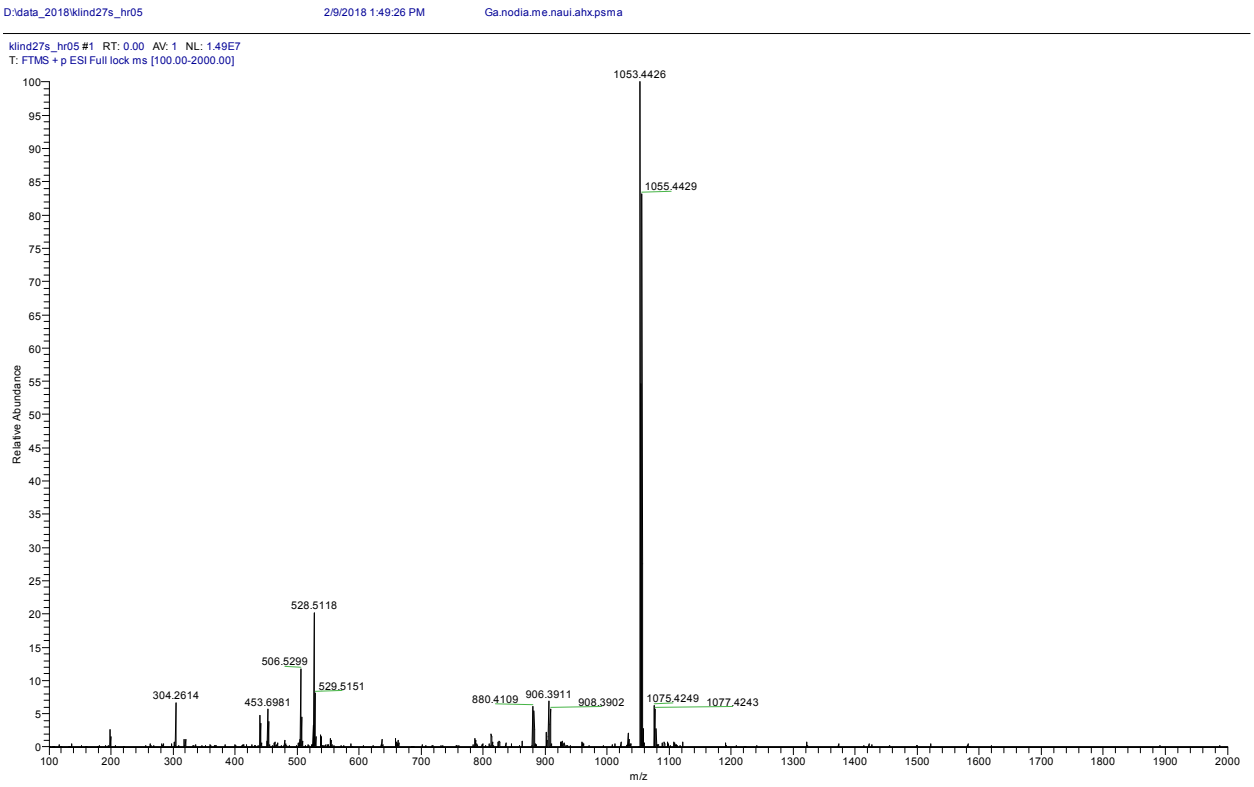

Figure S9. HR-ESI(+)-mass spectrum of Ga-**4**. Calc. for $[M - 2H]^+ = [C_{49}H_{68}N_{12}O_{10}Ga]^+ =$ 1053.4432.

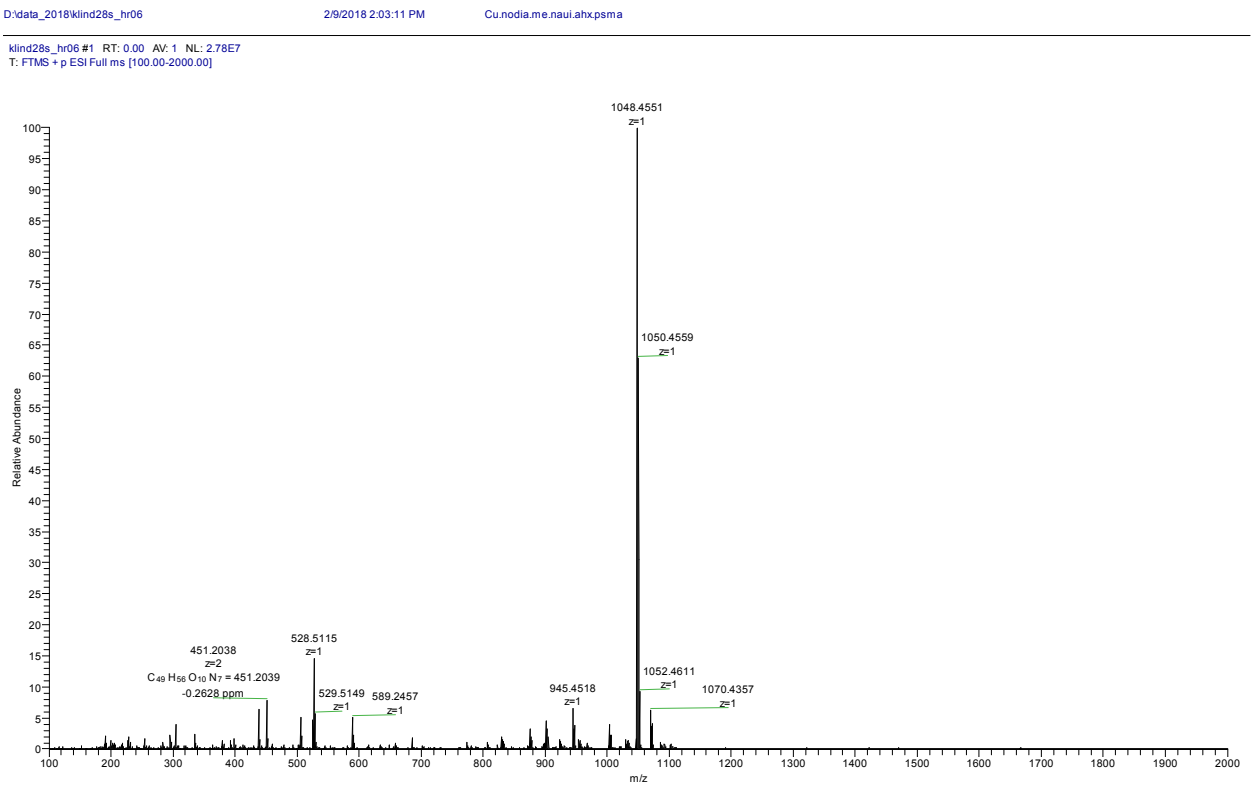

Figure S10. HR-ESI(+)-mass spectrum of Cu-**4**. Calc. for $[M - H]^+ = [C_{49}H_{69}N_{12}O_{10}Cu]^+ =$ 1048.4550.

HPLC chromatography

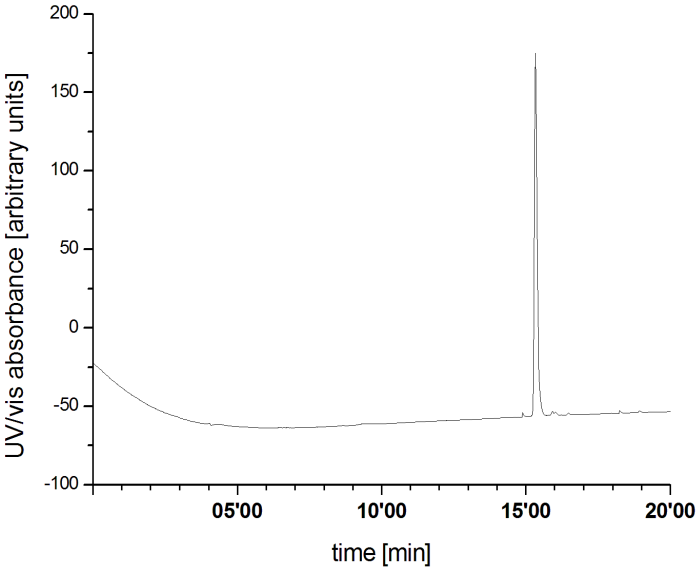

Figure S11. UV/vis trace of HPLC chromatogram of **4**.

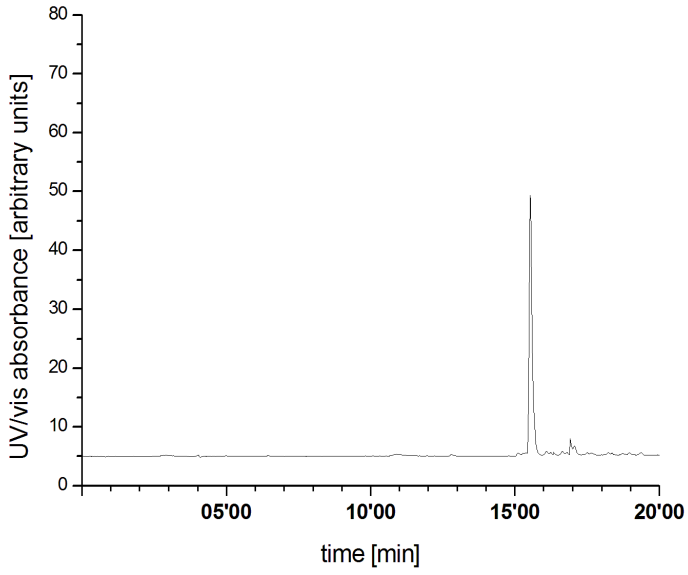

Figure S12. UV/vis trace of HPLC chromatogram of Ga-**4**.

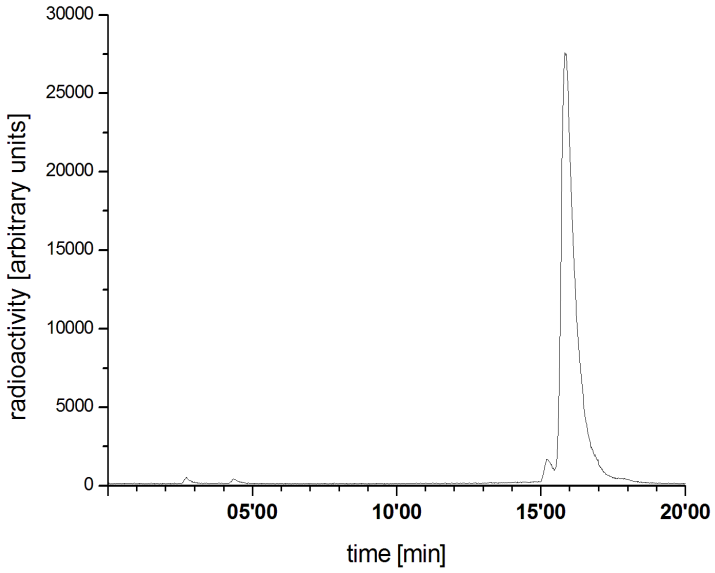

Figure S13. Radioactivity trace of HPLC chromatogram of [^{68}Ga]**4**.

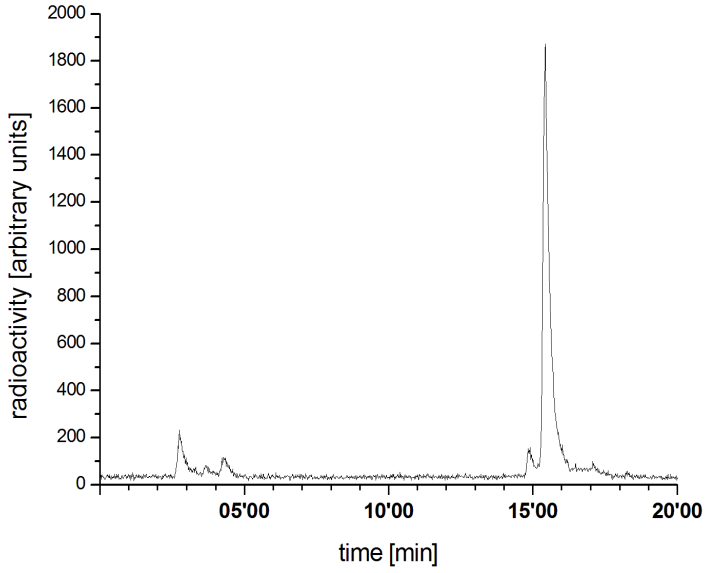

Figure S14. Radio-HPLC chromatogram of [^{68}Ga]**4** after 4 h incubation in human serum.

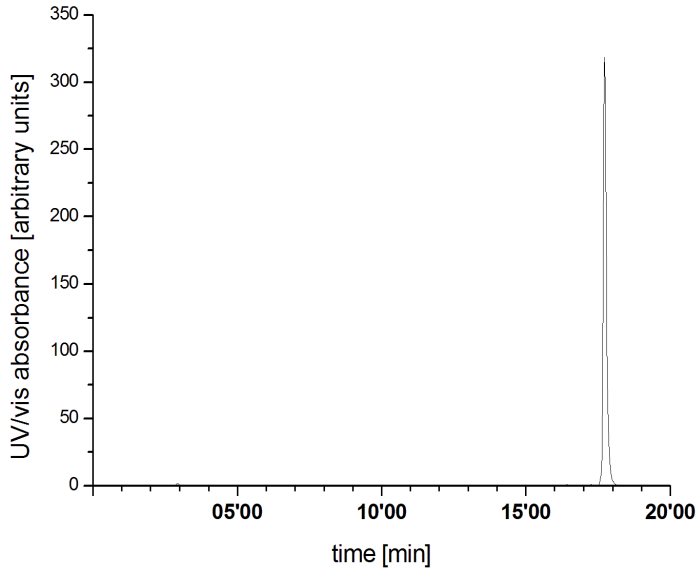

Figure S15. UV/vis trace of HPLC chromatogram of Cu-**4**.

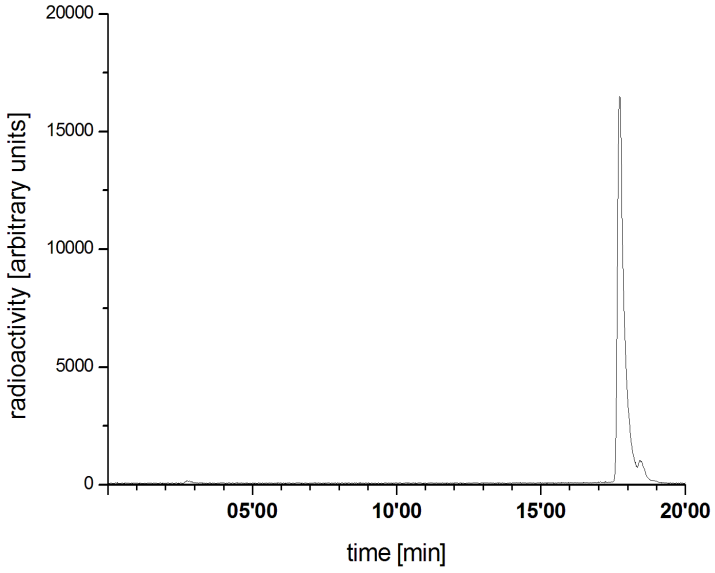

Figure S16. Radioactivity trace of HPLC chromatogram of [^{64}Cu]**4**.

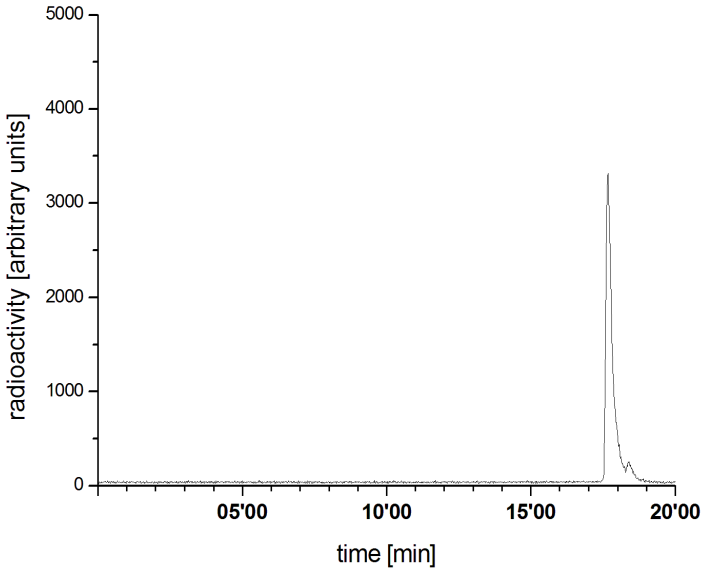

Figure S17. Radio-HPLC chromatogram of [^{64}Cu]**4** after 24 h incubation in human serum.

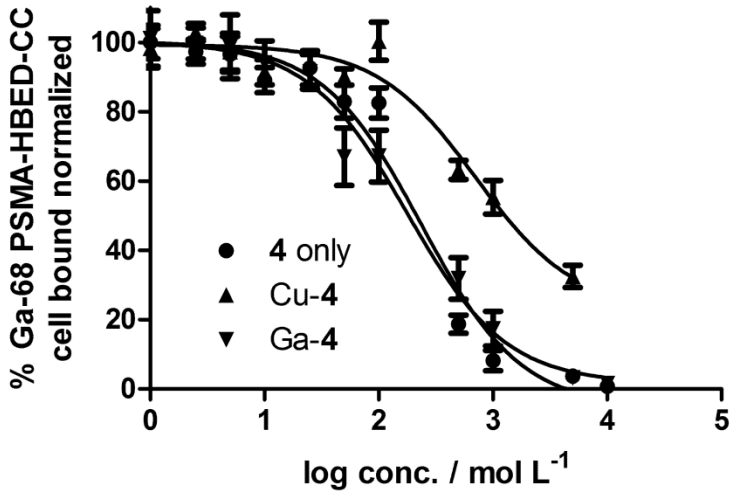

Figure S18. Determination of binding affinity of compounds **4**, Ga-**4** and Cu-**4** by competitive titration on LNCaP cells using [^{68}Ga]Ga-PSMA-HBED-CC as radioligand.